

CHAPTER IV

RESULTS AND DISCUSSION

4.1. Materials preparation and characterizations

4.1.1. OH-terminated lactic acid oligomer (PLA-glycolysate:GPLA)

PLA-glycolysate (GPLAs) with different MWs were obtained by varying the glycolysis conditions (Table 4.1). The biggest GPLA in the series, G44 (\bar{M}_n 44000 g/mol), was obtained by using a PLA:EG ratio of 1:0.5 (wt./wt.) at 175°C for 60 min. At higher temperatures and with the use of longer reaction times and higher EG contents, smaller-sized GPLAs were produced, i.e., G10 (\bar{M}_n 10000 g/mol) and G2 (\bar{M}_n 2000 g/mol). This indicates that the depolymerisation efficiency is strongly dependent on the EG content, and reaction temperature and time. This is in good agreement with those reported for the depolymerisation of its aromatic polyester counterpart, poly(ethylene terephthalate) (PET) [63].

The proposed-chemical structures of GPLAs examined by ^{13}C -NMR are presented in Figure 4.1. In cPLA (Figure 4.2), signals of in-chain methyl $-\text{OCH}_2\text{CH}_3\text{C}=\text{O}$ (C^a), terminal methyl $\text{HOCH}_2\text{CH}_3\text{C}=\text{O}$ (C^b), in-chain methine $-\text{OCHCH}_3\text{C}=\text{O}$ (C^d), and terminal methines $\text{HOCHCH}_3\text{COOCH}_2\text{CH}_3\text{C}=\text{O}$ (C^d) and $\text{HOCHCH}_3\text{C}=\text{O}$ ($\text{C}^{d'}$) are clearly observed at ~ 16.6 , 20.5, 68.9, 69.4, and 66.6 ppm, respectively. In addition, the carbonyl ($-\text{C}=\text{O}$) signal is observed at 169.6 ppm [64]. In contrast, GPLAs show additional signals at ~ 62.3 and 67.0 ppm, associated with EG terminals, i.e., $\text{O}=\text{COCH}_2\text{CH}_2\text{OH}$ (C^e), $\text{O}=\text{COCH}_2\text{CH}_2\text{OH}$ (C^f) [13]. This implies that GPLAs are comprised mainly of lactate repeat units, end-capped with hydroxyl groups (structure 4.1c). The signal at 60.6 ppm is assigned to methylene of in-chain EG units connected to PLA sequences ($-\text{OCH}_2\text{CH}_2\text{O}-$; C^g). The presence of these groups is a result from transesterification of polyester chains, leading to a formation of the structure 4.1d. In addition, the signals of EG and LA residues are observed in G2 products, obtained from the use of excess EG feed contents at 63.7 ppm, and 20.1, 66.4, and 173 ppm, respectively.



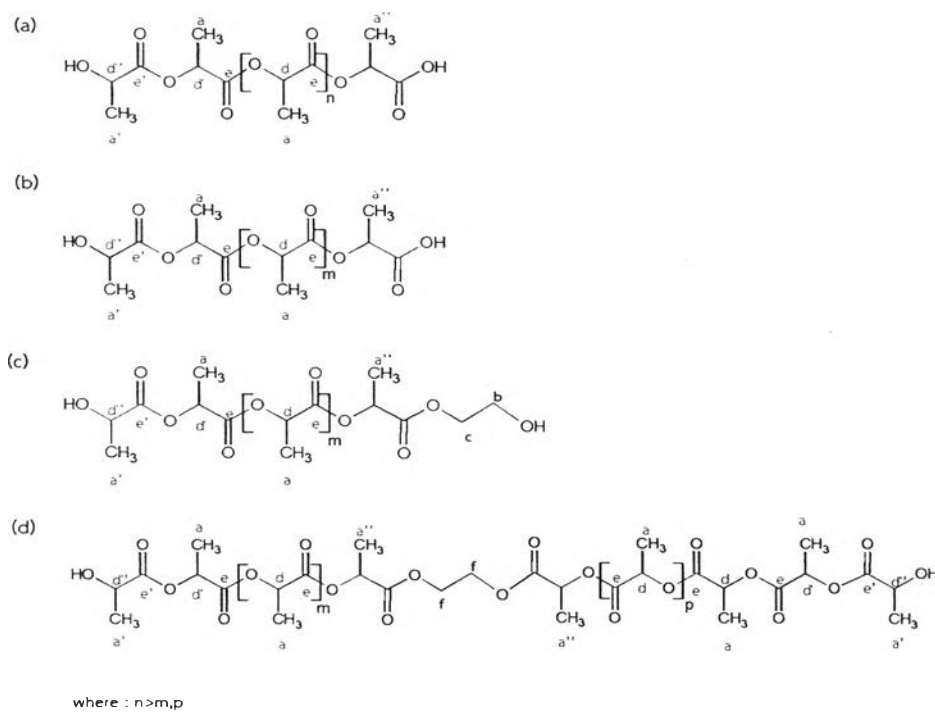


Figure 4.1 Chemical structures of CPLA (a) and propose chemical structure of GPLAs; LAA (b), LAB (c), and LAC (d).

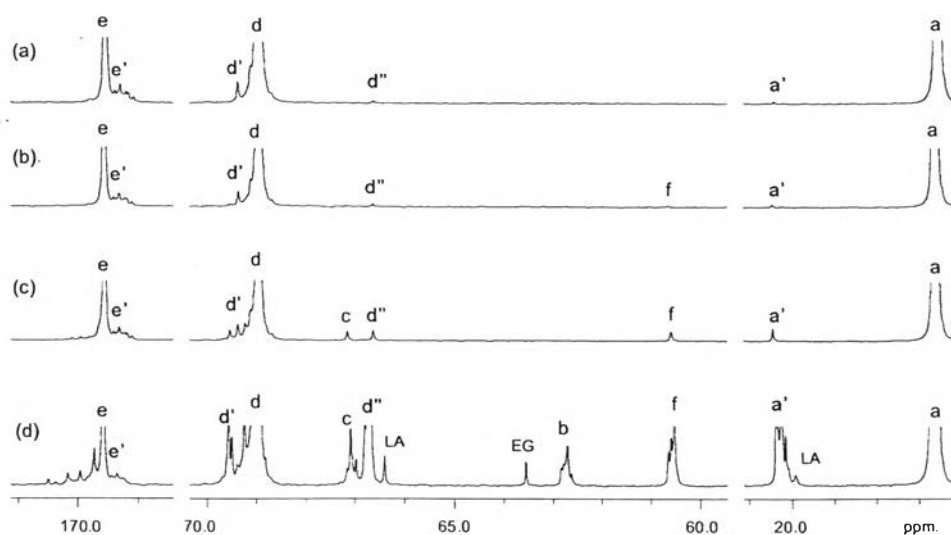


Figure 4.2 ^{13}C NMR spectra of cPLA (a), G44 (b), G10 (c), and G2 (d).

Table 4.1 Glycolysis conditions of PLA resin and properties of GPLA products.

Materials	Glycolysis conditions			GPC			MALDI-TOF			$\bar{M}_n \times 10^{-3}$ (g/mol) ^{13}C NMR	
	PLA:EG (wt/wt)	Temp (°C)	Time (min)	$M_n \times 10^{-3}$ (g/mol)	$M_w \times 10^{-3}$ (g/mol)	PDI	$\bar{M}_n \times 10^{-3}$ (g/mol)	Structure (%)			
								(a)	(b)		(c)
cPLA	-	-	-	140	190	1.35	-	-	-	-	-
G44	1 : 0.5	175	60	44	77	1.75	7.9	34	58	9	15
G10	1 : 0.5	195	60	10	18	1.77	2.1	21	71	9	5.1
G2	1 : 1	195	30	2	3	1.37	1.7	40	60	-	0.4

MALDI-TOF mass spectra of GPLAs are shown in Figures 4.3-4.5. G10 spectrum (Figure 4.4) shows 3 major peak series, whose m/z intervals equal to molar mass of lactate repeating units ($M = 72$). The most intense peak series (more than 71%) are associated with oligomers doped with Na^+ ions of type $\text{H} \cdot [\text{LA}]_n \cdot \text{CH}_2\text{CH}_2\text{OH} \cdot \text{Na}^+$ ($m/z = 72n+1+61+23$). This is derived from GPLA structure 4.1b, i.e., LA oligomers containing $-\text{OH}$ and $-\text{CH}_2\text{CH}_2\text{OH}$ terminals. Two other intense mass series are observed at $m/z = 72n+1+17+23$ and $m/z = 72n+1+17+60+23$, which correspond to Na^+ doped species of GPLA structures 4.1a (21%) and 4.1c (9%), respectively. This confirms the proposed structures of products from the glycolysis reaction of PLA. G44 spectrum (Figure 4.5) also shows similar peak series, but with higher relative peak intensity of structures 4.1b. This indicates relatively higher contents of structures 4.1b and 4.1d, when bigger-sized GPLA are produced. In contrast, the corresponding spectrum of G2 (Figure 4.3) shows a major characteristic of structure 4.1c (60%), with that of structure 4.1b as an only minor constituent (40%). The absence of the peak series associated with structure 4.1d in this small-sized GPLAs and the variation of its relative intensity in bigger-sized GPLAs indicate that the formation of structure 4.1c occurs at an early stage of glycolysis, or at mild glycolysis conditions, presumably by trans-esterification. With an increase of glycolysis times or temperatures, the generation of this structure

is retarded. Most importantly, the employment of an excess amount of EG in feed, i.e., a PLA:EG ratio of 1:1 compared to 1:0.5 (Table 4.2), leads to a formation of low-MW GPLAs and a reduction of structure 4.1c content.

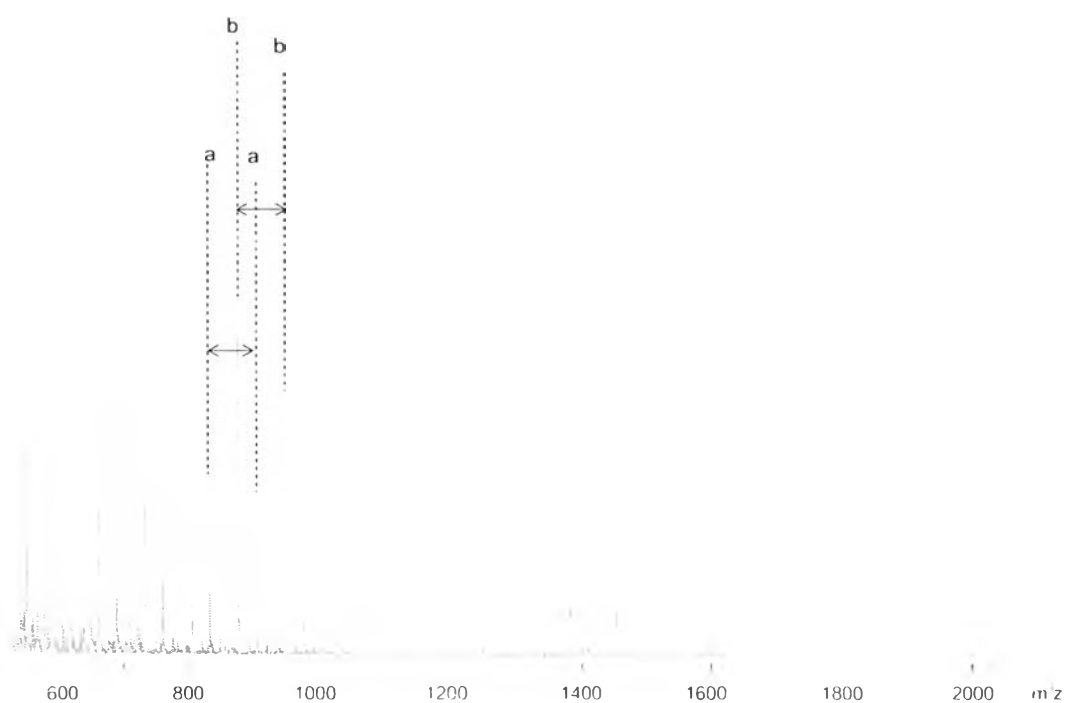


Figure 4.3 MALDI-TOF Mass spectrum of G2.

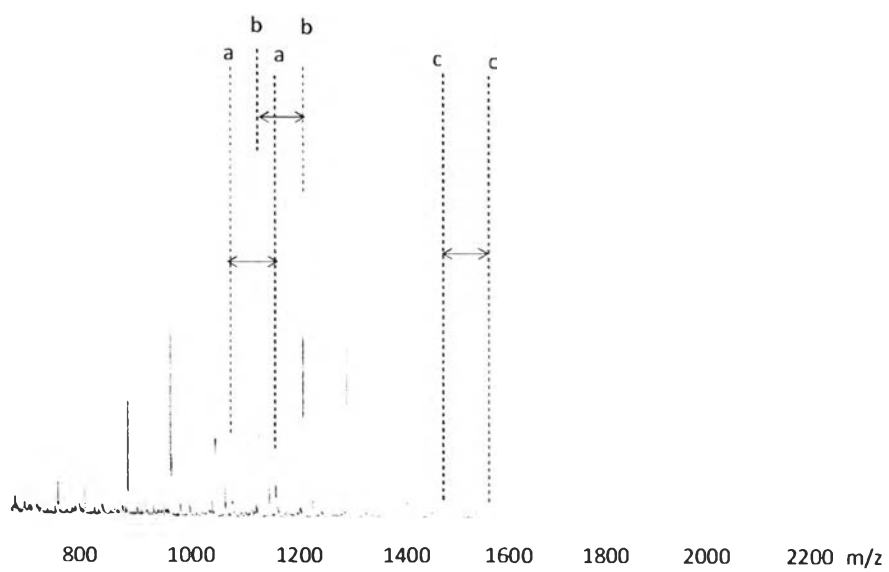


Figure 4.4 MALDI-TOF mass spectrum of G10.

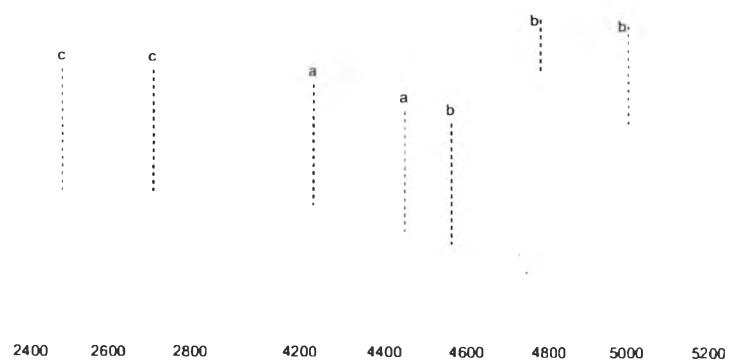


Figure 4.5 MALDI-TOF mass spectrum of G44.



Interestingly, the calculated \overline{M}_n values, from MALDI-TOF mass spectra, are much lower than those obtained from GPC and ^{13}C -NMR experiments (Table 4.2). It was reported that MALDI-TOF MS was not suitable for determination of average molecular weight of polymers with a polydispersity of 1.2 or higher, as large-chain components are usually underrepresented, compared to lower mass oligomers [60]. This was caused by several factors, such as, sample preparation, mass-dependent desorption/ionization process, and mass-dependent detection efficiency. Nevertheless, it is noted that deviations of the results obtained from GPC may also be observed, as this technique analyzes the samples based on their hydrodynamic volume in comparison with those of polystyrene standards [59].

Table 4.2 Glycolysis conditions of PLA resin and properties of GPLA products.

Materials	Glycolysis conditions			GPC			MALDI-TOF			$\overline{M}_n \times 10^{-3}$ (g/mol) ^{13}C NMR	
	PLA:EG (wt/wt)	Temp (°C)	Time (min)	$\overline{M}_n \times 10^{-3}$ (g/mol)	$\overline{M}_w \times 10^{-3}$ (g/mol)	PDI	$\overline{M}_n \times 10^{-3}$ (g/mol)	Structure (%)			
								(a)	(b)		(c)
cPLA	-	-	-	140	190	1.35	-	-	-	-	-
G44	1:0.5	175	60	44	77	1.75	7.9	34	58	9	15
G10	1:0.5	195	60	10	18	1.77	2.1	21	71	9	5.1
G2	1:1	195	60	2	3	1.57	1.7	40	60	-	0.4

ATR-FTIR spectra of GPLAs are presented in Figure 4.6. Characteristic band of in-chain lactate units is observed at 1080 cm^{-1} (C-O-C stretching). The C=O stretching modes of free C=O is observed at 1770 cm^{-1} , whereas those of hydrogen bonded groups are located at 1755 and 1750 cm^{-1} .

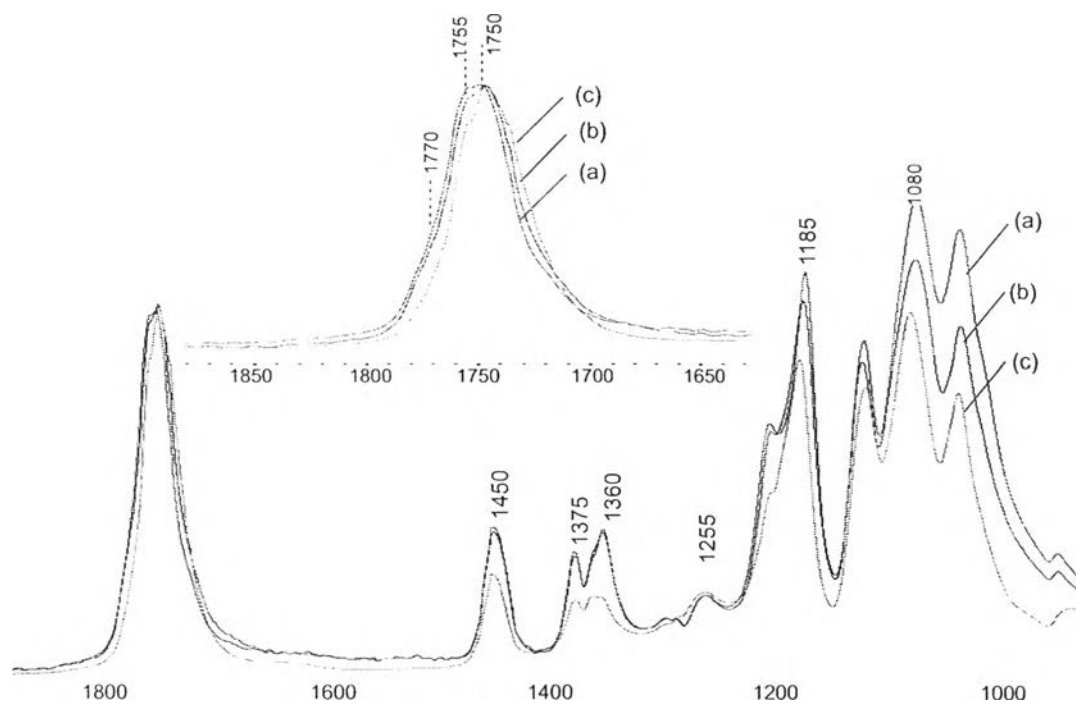


Figure 4.6 ATR-FTIR spectra of G44 (a), G10 (b), and G2 (c).

The band frequency indicates the strength of hydrogen bond interaction, in which that at lower frequencies is corresponding to stronger interaction. The intensity of the 1755 cm^{-1} mode decreases with a decrease in MW of the products, i.e., higher contents of -OH groups from EG terminals. In contrast, the 1750 cm^{-1} band increases in intensity, with an increase in the degree of glycolysis. This indicates that GP_{As} with lower MW contains higher relative content of OH groups, leading to higher degree of hydrogen bonding. Further shift of the band is observed in G2, where the vibrational mode at low frequency presents as a shoulder band. The C=O band-normalized spectra show that the intensity of a 1080 cm^{-1} mode varies with the degree of glycolysis. This indicates a conversion of lactate esters to free carboxylic acid end-groups.

TGA and DTGA thermograms of cPLA and GPLAs are shown in Figure 4.7. Thermal degradation of PLA glycolysates main chains involves a one-step degradation. The cPLA resin shows a narrow thermal-degradation profile, whereas GPLAs show a broader degradation pattern, due to a relatively higher OH end-group contents of GPLA, compared to commercial PLA. These groups can form hydrogen bond with carbonyl groups. G2 shows the lowest degradation temperature (T_d) and onset temperature (T_{onset}) (Table 4.3) because of a low crystallinity of its short chain structure. In contrast, longer GPLAs (G10 and G44) show higher T_d at 345°C and 360°C, respectively.

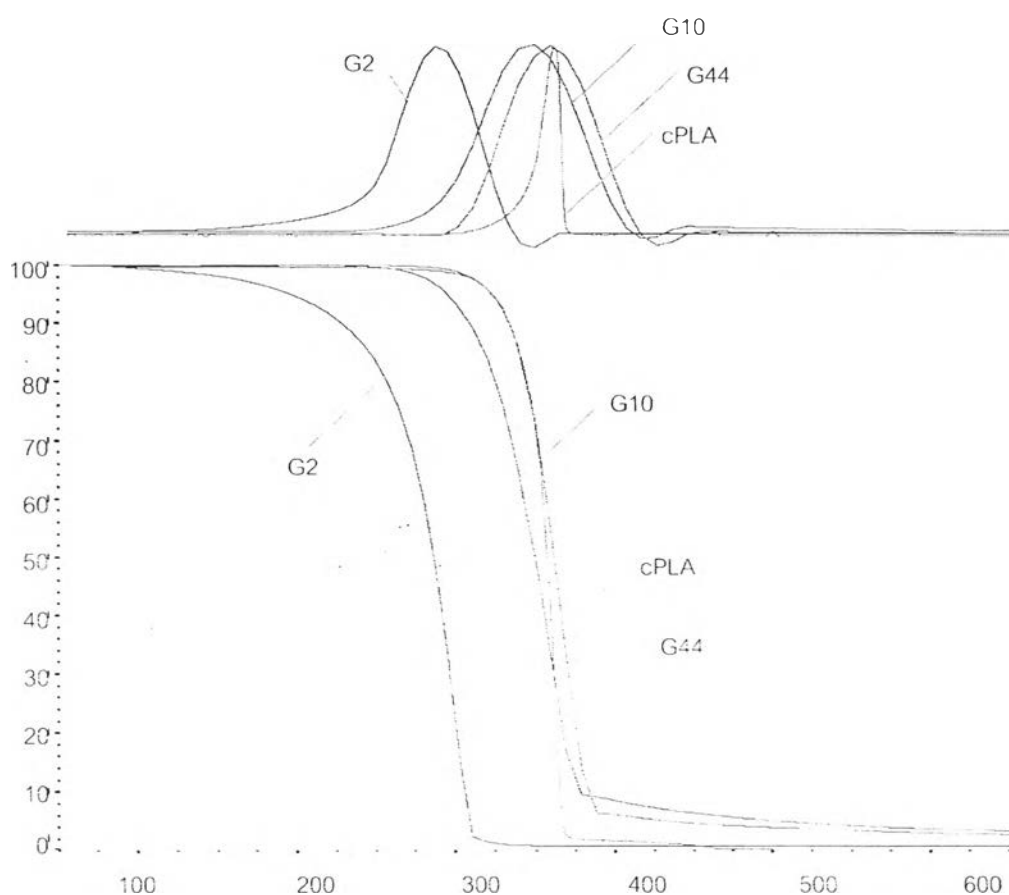


Figure 4.7 TGA and DTGA thermograms of commercial PLLA and GPLAs.

Table 4.3 Thermal properties of commercial PLA and GPLAs.

Materials	DSC			TGA	
	T_g^a	T_m^b	ΔH_f^b	T_{onset}	T_d
cPLA	68	-	-	320	360
G44	60	153	45.6	320	360
G10	52	148	45.6	280	345
G2	-10	92	41.5	150	300

^a : data from 2nd heating scan

^b : data from 1st heating scan

4.1.2. Analysis of Epoxidized natural rubber (ENR)

Epoxidation of NR latex was carried out by reacting with hydrogen peroxide and formic acid. Chemical structure of the resulting ENR was analyzed by ¹H NMR and ATR-FTIR spectroscopy. ¹H-NMR spectrum of ENR (Figure 4.8) shows signals at 1.67, 5.1 and 2.16 ppm, assigned to methyl (H^a), methine (H^b) and methylene (H^c) protons of cis-1,4-polyisoprenic structure, respectively. The signals of methyl (H^d), methine (H^e), and methylene (H^f) groups adjacent to epoxide units are observed at 1.26, 2.7 and 1.5 ppm, respectively [65]. The degree of epoxidation, determined from the integration ratio of the methine proton adjacent to oxirane ring at 2.7 ppm and the proton adjacent to C=C of polyisoprene at 5.1 ppm, is 20%. FTIR spectrum of ENR, as shown in Figure 4.9(a), reflects characteristic signals of epoxide ring at 1250 cm⁻¹ (symmetric stretching) and 870 cm⁻¹ (asymmetric stretching) [7].

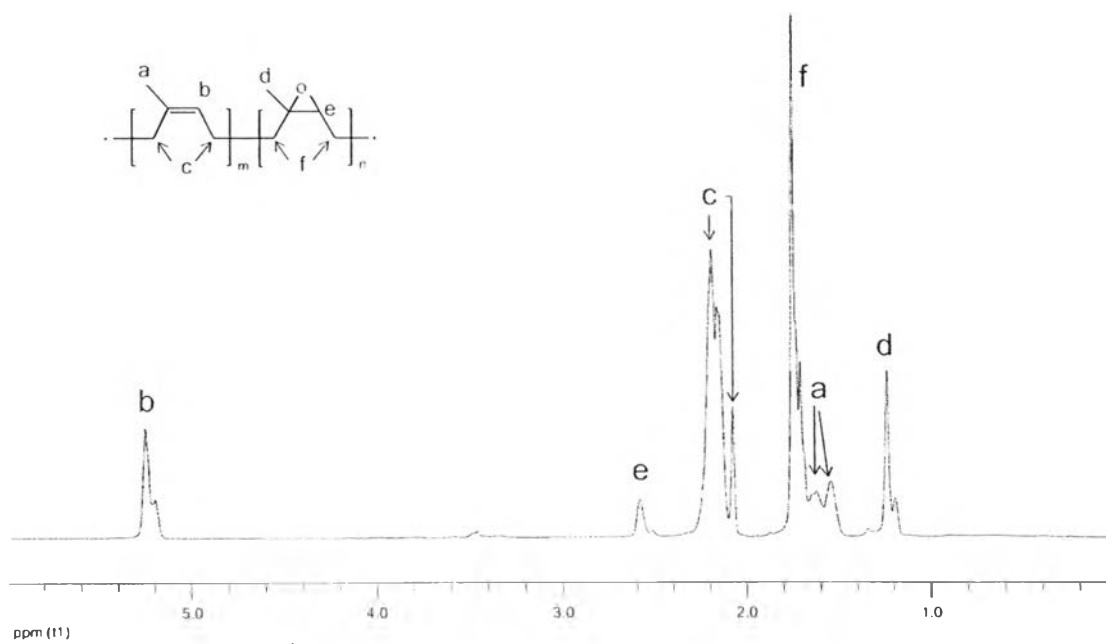


Figure 4.8 ^1H NMR spectrum and chemical structure of ENR.

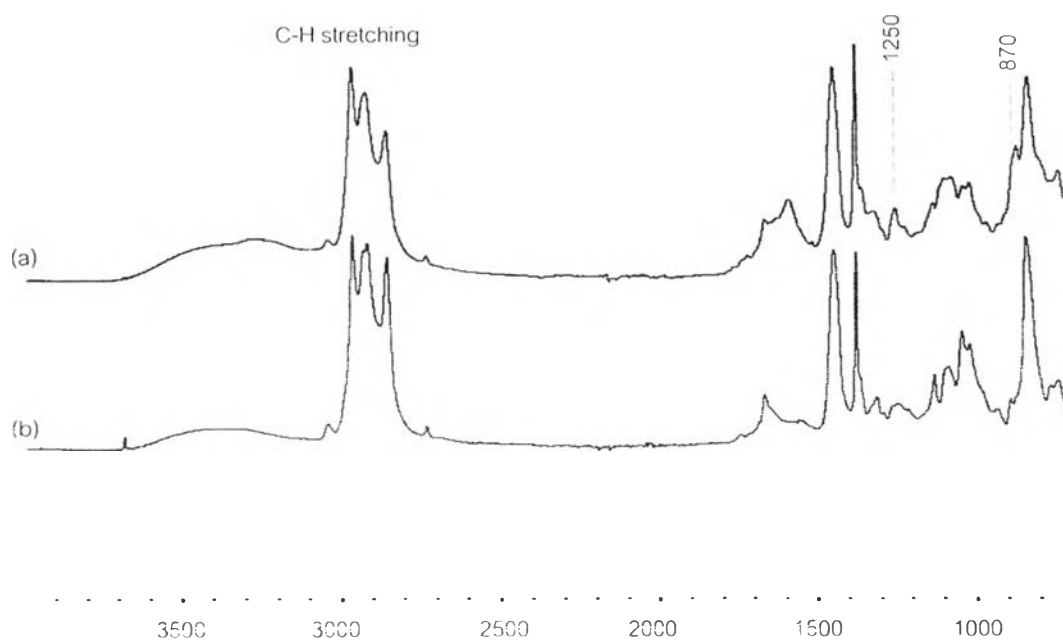


Figure 4.9 ATR-FTIR spectra of ENR (a) and NR (b).

4.2. Preparation of GPLA-cured ENR materials

GPLA-cured ENR materials in this work were prepared by three different procedures, i.e. chemical curing in solution (according to 3.5.1), reactive crosslinking in MDR (according to 3.5.2) and in an internal mixer (according to 3.6.5). The results from the chemical reactions (in solution) and reactive crosslinking (MDR) methods provide in-depth information on curing mechanisms and chemical structures of the cured ENR products. In parallel, the reactive melt blending method is more practical for industry. Details on these curing approaches are describes in sections 4.2.1-4.2.4.

4.2.1. Curing characteristic of ENR and NR

Crosslinking efficiency of ENR by GPLA (G44) crosslinkers is examined, in comparison with NR. A reactive curing process was carried on a Moving Die Rheometer (MDR) at 80 °C for 30 min. Figure 4.10 shows elastic torque values of ENR-GPLA and NR-GPLA mixtures, as a function of curing times, with a variation in rubber:GPLA weight ratios. The samples are denoted by the name of the corresponding GPLA, and ET for ENR or NT for NR, respectively. G44ET and G44NT are examined. Scorch times for the curing of both ENR and NR samples are shorter than 5 min, which is in the same range as those of typical sulfur-vulcanized ENR and NR (~ 2 and 4 min, respectively) [66]. When the G44 loading content increases, the curing rate of both ENR and NR mixtures increases. This is likely because the hydroxyl end groups in G44 plays an important role on the progress of the crosslinking reaction, as reported by Nakason et al. [67]



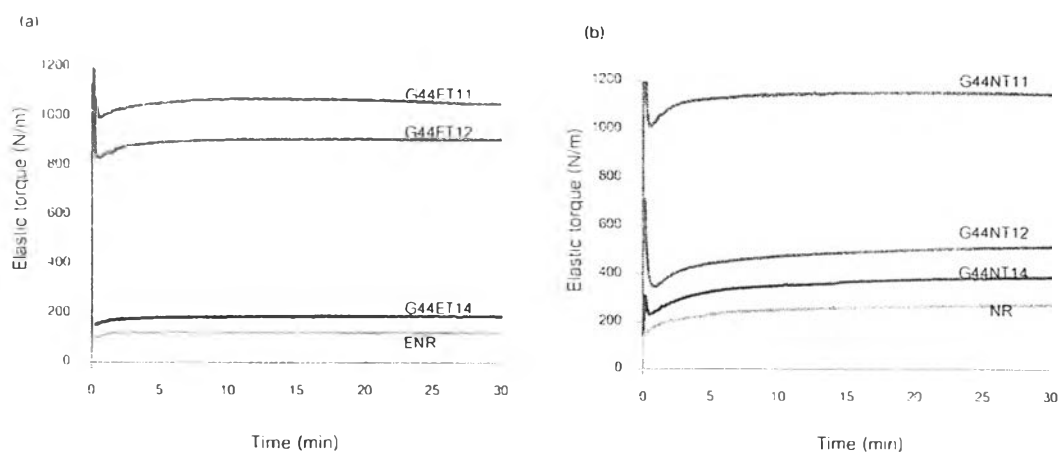


Figure 4.10 Plots of elastic torque, as a function of curing time, of G44/ENR mixtures (a) and G44/NR mixtures (b), prepared at different rubber/GPLA ratios.

The minimum torque (M_L) values of both ENR-based and NR-based mixtures increase with an addition of GPLA, compared to neat ENR and NR. Since M_L is regarded as stock viscosity, this implies that the incorporation of polymers increases the viscosity of both ENR and NR rubbers [68]. A similar trend is also observed for the maximum torque (M_H), where the values increase with an increase in the polymer loading content. This is because M_H is correlated to modulus of the mixtures [67, 69]. An incorporation of polymers in rubber matrix increases the rubber modulus, as a result from the restriction of its chain flexibility. The observed lower elastic torque value of pure ENR, compared to pure NR, is mainly due to an extensive main-chain modification caused by the reduction in molecular weight of NR, as a result from side reactions of the epoxidation process [70]. M_H value of G44ET11 is significantly similar to that of G44NT11, due to a domination effect of excess GPLA (50 wt%). Similarly, M_L values of G44ET14 and G44NT14 are not significantly different, as these samples are also dominated by rubber domains with low content of hydroxyl groups. In contrast, M_H values of G44ET12 are clearly higher than those of G44NT12. This indicates that a G44:ENR weight ratio of 1:2 is an optimum composition for crosslinking of ENR, which is not appropriate in the less reactive NR mixture.

The viscous torque of rubber mixtures also increases with an increase in G44 composition, as shown in Figure 4.11. This is probably because an excess amount of unreacted species, i.e., a “simple blend” fraction, increases the flow characteristic of the mixture, reflecting in an increase of the viscous torque or damping behaviors of pure rubbers. These results indicate that the contents of crosslinked domains and “simple blend” fraction play a major role in the viscoelastic behaviors of the blends.

The efficiency of crosslinking reaction is reflected by the time-dependent loss tangent ($\tan \delta$) values of the blends, as shown in Figure 4.12. This is calculated from a ratio of viscous torque to elastic torque, where the low values indicate high elasticity. Conversely, large $\tan \delta$ values indicate high degree of viscous behaviors. The loss tangent values of ENR mixtures are lower than neat ENR, indicating that the incorporation of G44 increases the elasticity of ENR, as a result of the crosslinked network structure formation. On the other hand, all NR/G44 mixtures show higher $\tan \delta$ values than pure NR. This confirms a very low crosslinking content in the epoxide-deficit rubber samples. The higher $\tan \delta$ values of G44ET11 and G44NT11, compared to the corresponding samples at a ratio of 1:2, might be due to a domination of excess GPLA characteristics.

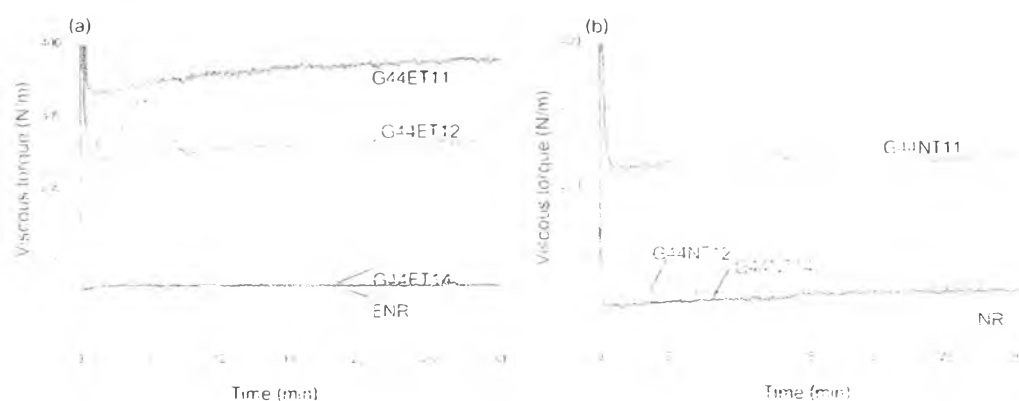


Figure 4.11 Plots of viscous torque, as a function of curing time, of G44/ENR mixture (a) and G44/NR mixtures (b), prepared at different rubber/GPLA ratios.

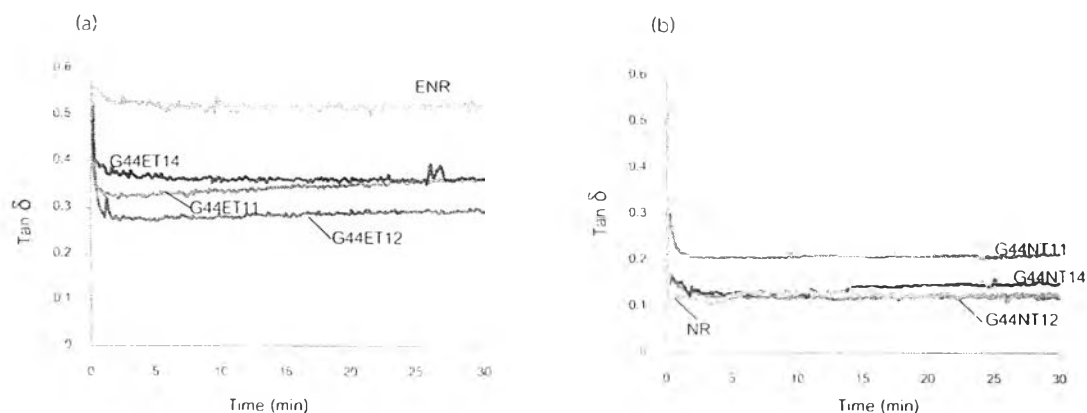


Figure 4.12 Plots of $\text{Tan } \delta$, as a function of curing time, of G44/ENR mixture (a) and G44/NR mixtures (b), prepared at different rubber/GPLA ratios.

Table 4.4 Weight percentage of extracted fractions obtained from sequential solvent fractionation, degree of swelling, and gel contents of G44ET14 and G44NT14 blends.

Sample	Composition in feed (wt%)			Weight fraction (%)			Gel content (%)	Swelling ratio (%)
	G44	ENR	NR	S_{THF}	S_{Tol}	I_{Tol}		
G44ET14	20	80	-	41±2	21±2	39±4	65±2	1648±10
G44NT14	20	-	80	76±2	17±1	17±2	50±3	850±9

Table 4.4 summarizes weight percentage of extracted products of ENR and NR cured samples. The content of S_{THF} of G44ET14 is 41%, while S_{Tol} and I_{Tol} are about 21 and 39 wt%, respectively. As free GPLA and neat ENR can completely dissolve in THF and toluene, the content of I_{Tol} fraction confirms the presence of chemically-modified structures, i.e., a cured network which is non-soluble. The percentage of soluble fractions (both S_{THF} and S_{Tol}) of G44NT14 are about 83 wt%, compared to 80% NR feed content. The difference is likely a result of the relative difference in their solubility parameters (δ_v). As THF soluble G44 is accounted for 20 % of the value, this indicates that NR ($\delta_{\text{NR}} = 8.2 \text{ (cal/cm}^3)^{1/2}$) can dissolve in both THF ($\delta_{\text{THF}} = 9.1 \text{ (cal/cm}^3)^{1/2}$) and toluene ($\delta_{\text{Tol}} = 8.9 \text{ (cal/cm}^3)^{1/2}$).

Degree of crosslinking of the cured products is determined from toluene extraction of the remaining THF-insoluble fraction, at room temperature for 7 days. Table 4.4 show a gel content of cured ENR sample is 65%, while that of the corresponding NR sample is 50%. However, the I_{Tot} weight fraction of G44NT14 is only half of that of G44ET14 (17% and 38%). This confirms the crosslinking reaction of ENR by G44, whereas conventional crosslinking also slightly occurs in the NR mixture.

The crosslinking density of the I_{Tot} samples are recorded in term of a swelling percentage of the sample in toluene, as also summarized in Table 4.4. The swelling ratio of the cured fraction of G44NT14 is about 850%, which is in the same range as those of typical sulfur-vulcanized NR (~ 800%) [9]. This reflects that crosslinking by other mechanisms may slightly occur during the MDR experiment, due to high temperature and the applied shear force. In contrast, the corresponding sample of G44ET14 exhibits very high swelling ability (higher than 10 times of their original dimensions), and about 2 folds higher than that of the NR counterpart. This strongly supports our proposed crosslinking mechanisms, as stated earlier, in which G44 chains act as long-chain bridges, providing higher flexibility for the cured rubber network swelling.

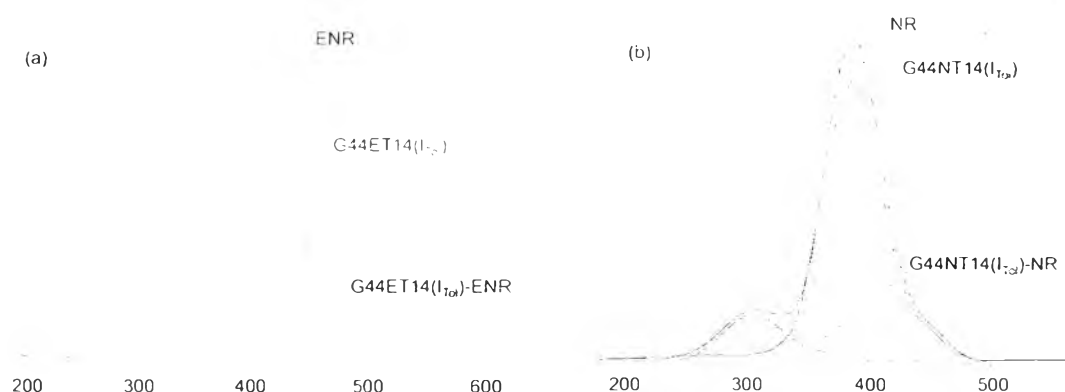


Figure 4.13 DTGA thermograms of toluene-insoluble fraction obtained from G44ET14 (a) and G44NT14 (b) cured products.

DTGA thermograms of I_{rot} fraction of G44ET14 and G44NT14 cured samples are compared to those of their corresponding neat ENR and NR in Figure 4.13. Pure ENR and NR show a single DTGA peak at around 400°C, indicating that thermal degradation of these raw materials is mostly a one-stage process due to their homogeneous nature. The degradation characteristic of G44ET14 and that after subtraction of neat ENR (G44ET14-ENR) are shown in Figure 4.13(a). The subtracted thermogram exhibits 3 steps of degradation. A low temperature peak observed at approximately 300°C, is attributed to the degradation of grafted lactate units on ENR domain. A second step, observed between 350°C to 400°C, is the degradation of lactate block sequences that act as crosslinked chains on ENR backbones, whereas the mass loss step observed at 450°C is likely due to the loss of by-products, i.e., crosslinked and cyclized networks of rubber domains [71]. In contrast, the subtraction result from G44NT14-NR, as shown in Figure 4.13(b), exhibits only one degradation peak at approximately 300°C attributed to small amounts of lactate block sequences, which are crosslinked to rubber domains under dynamic crosslinking conditions. This is because free radicals are produced on carbon atoms at the allylic positions of NR, to initiate the crosslink reaction [72].

4.2.2. GPLA-cured ENR via chemical crosslinking reaction (GER)

4.2.2.1. Chemical structure of GER products

Chemical structures of GPLA-cured ENR products obtained from chemical reactions of ENR and GPLA in a clean reactor and purified-solvent are proposed in Figure 4.14-4.15. Three proposed structures of GPLA-cured ENR products, i.e., “crosslinked”, “grafted”, and “simple blend”, were sequentially fractionated by solvent extraction and their properties were characterized.

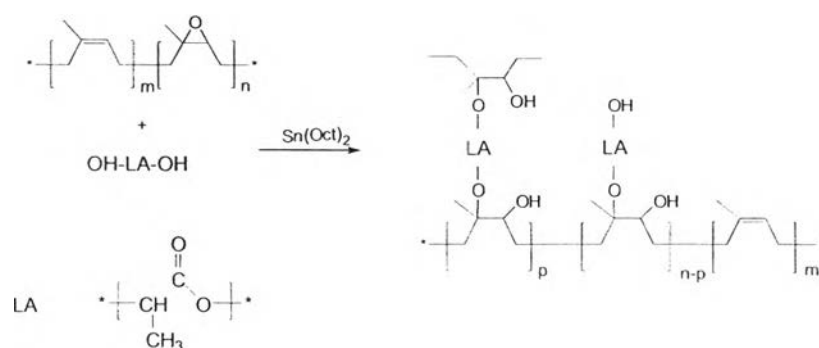


Figure 4.14 Crosslinking reaction of ENR by GPLA macromolecular crosslinker.

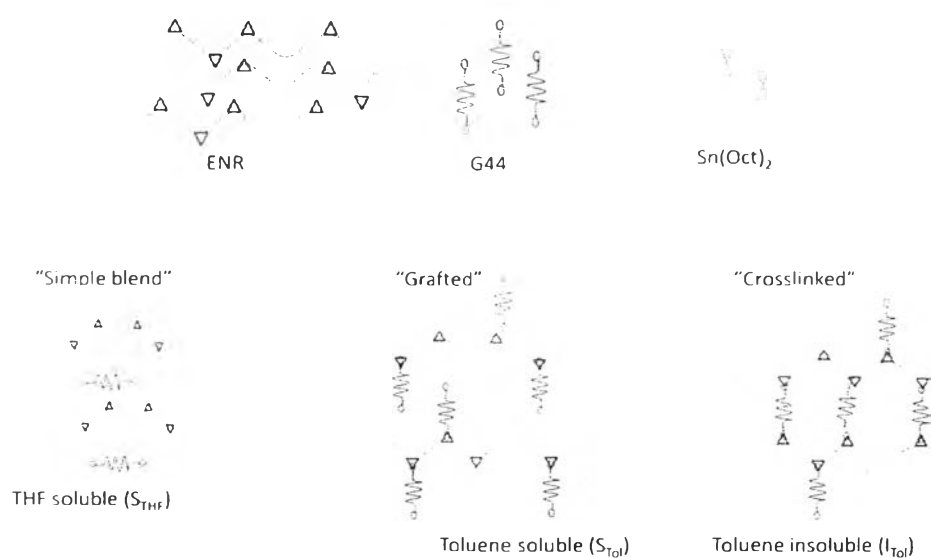


Figure 4.15 Possible structures of GPLA-cured ENR products and their solvent solubility.

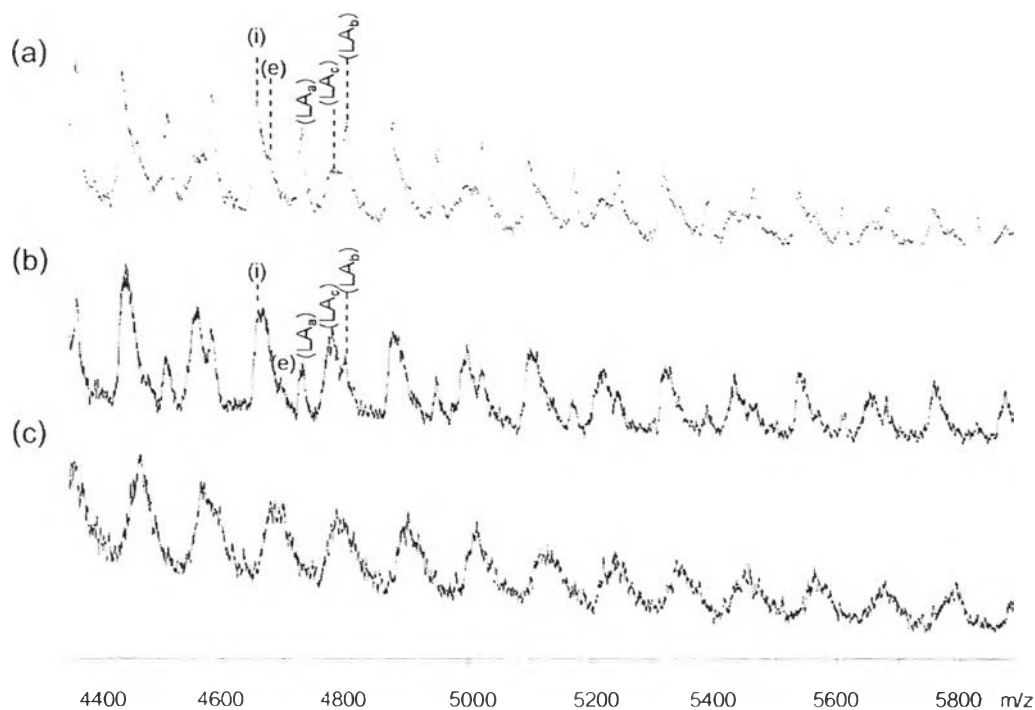


Figure 4.16 MALDI-TOF mass spectra of G10ER11(S_{THF}) (a), G10ER11(S_{Tol}) (b), and ENR (c) in a range of 4300 - 5900 m/z.

MALDI-TOF mass spectra of G10-cured ENR products are compared with pure ENR, as shown in Figure 4.16. The spectra were obtained using ditranol as a matrix and Silver trifluoroacetate (AgTFA) doping agent. Chemical structures of the “simple blend” fraction of G10ER11 (Figure 4.16a) exhibits both free GPLA (structure LA_a , LA_b , and LA_c) and unreacted ENR, i.e., isoprene units (i) and epoxide units (e). Mass of epoxide unit (e) is higher than that of isoprene unit (i) about 16 Da, due to its oxygen atom. The pattern of LA units in “simple blend” fraction, i.e. S_{THF} , is also clearly observed. Nonetheless the results confirm that the dissolved product after soxhlet extraction by THF solvent is free ENR and unreacted GPLA.

Similar to the “simple blend” fraction, the “grafted” fraction, which is soluble in toluene, exhibits 5 mass peak series (Figure 4.16b). The mass values of LA units in the “grafted” fraction is 1 Da lower than those in the free LA fraction, likely due to an absence of a hydrogen atom from GPLA chain end as a result from the grafting reaction. This, in turns, leads to a mass increase of epoxide group from an addition of

a hydrogen atom after ring-opening reaction, as shown in Figure 4.17. Signals of LA_b and LA_c show different relative intensity to that of the S_{Tot} fraction. The decrease in the LA_b signal reflect that grafting of GPLA on ENR is more likely due to EG's hydroxyl end groups than lactate hydroxyl terminal.

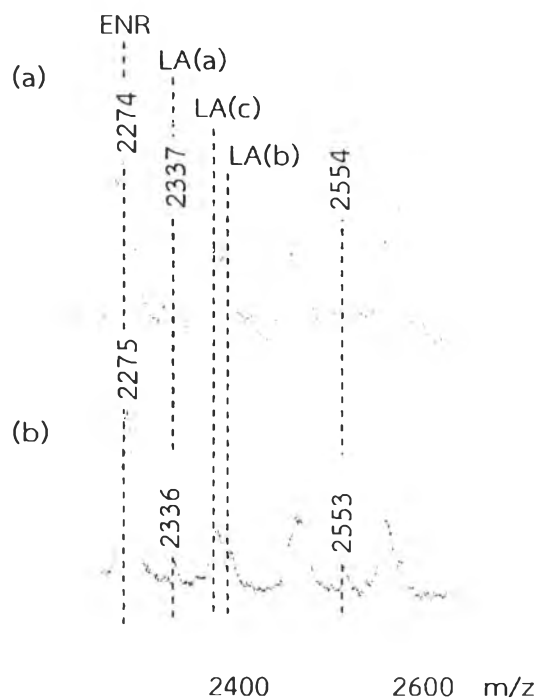


Figure 4.17 MALDI-TOF Mass spectra of G10ER11(S_{THF}) (a), G10ER11(S_{Tot}) (b) in a range of 2200 - 2700 m/z .

Figure 4.18 shows the corresponding mass spectra in full scale, where the peak series with the highest intensity are labeled. The "grafted" structure shows the highest maximum mass values, compared to free ENR and the "simple blend" fraction. This implies that grafting and crosslinking reaction (which low crosslinking efficiency) take place and generate products with higher mass.

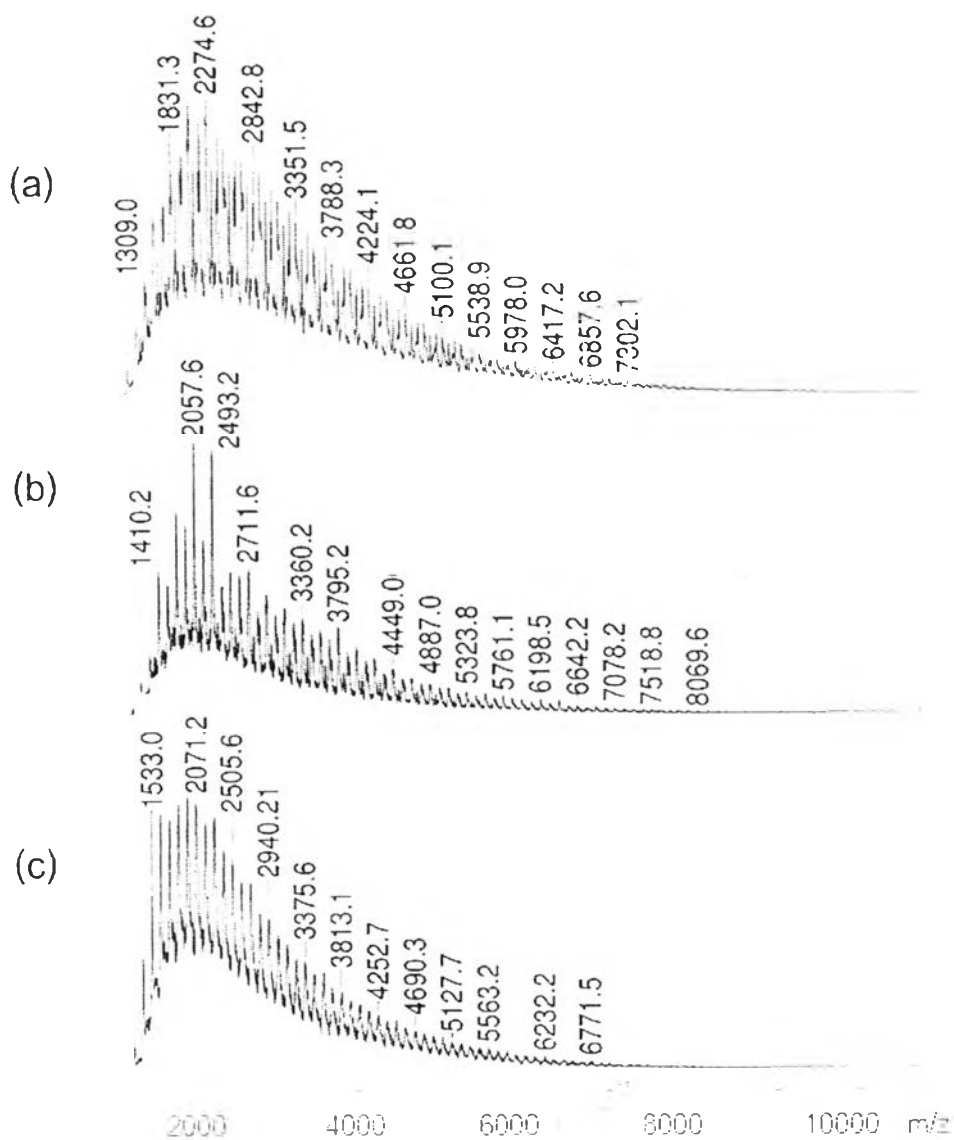


Figure 4.18 MALDI-TOF mass spectra (full scale) of G10ER11(S-THF) (a), G10ER11(S-THF) (b), and ENR (c).

Chemical structures of the “simple blend” and “grafted” soluble fractions are characterized by $^1\text{H-NMR}$ spectroscopy, as shown in Figure 4.19. The characteristic signals of ENR and G10 are clearly observed in the 2 extracted products. This indicates that the G10 “grafted” ENR fraction, with low grafting efficiency, can be slightly dissolved in THF solvent.

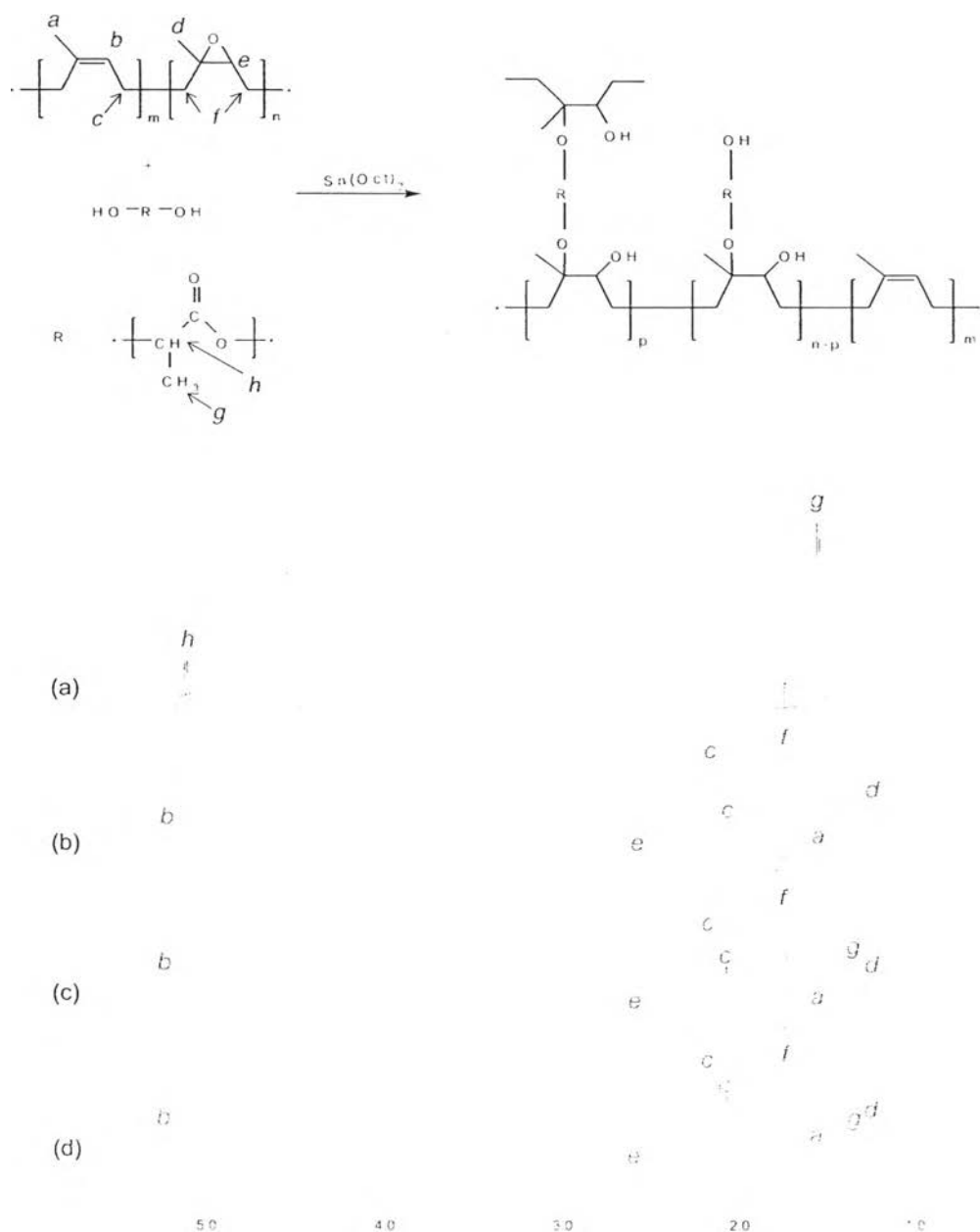


Figure 4.19 $^1\text{H-NMR}$ spectra of G10 (a), ENR (b), G10ER11(S_{7f}) (c), and G10ER11(S_{7g}) (d).

Mechanism of the chemical crosslinking reaction of ENR by GPLA crosslinkers (using a GPLA:ENR ratio of 4:1) is examined by FTIR spectroscopy. FTIR spectra of the samples are normalized against the characteristic band of rubber units at 1655 cm^{-1} ($\text{C}=\text{C}$ stretching) [7, 69]. Changes in intensity of the 1750 cm^{-1} mode ($\text{C}=\text{O}$ stretching of lactate) are then quantitatively analyzed [73], as shown in Figure 4.20-4.22

The normalized spectra of a G10ER14 mixture at 80°C are recorded as a function of time. The characteristic band of lactate units increases in intensity with time, as shown in Figure 4.20. As the spectra are recorded in ATR mode, the spectra only represent characteristic of surface of the film, with a penetration depth of about 200 μm . In an early stage of reaction, i.e., time of 0 hour, an immiscible mixture of the 2 components is measured. GPLA forms droplets and slowly disperses into ENR matrix as a function of reaction time. Consequently, “crosslinked” and “grafted” fractions are generated and act as stabilizer or compatibilizer, leading to formation of fine droplets of unreacted GPLA. Finally, GPLA domains homogeneously dispersed in ENR matrix, resulting an increase in intensity of the 1750 cm^{-1} mode, as a function of time.

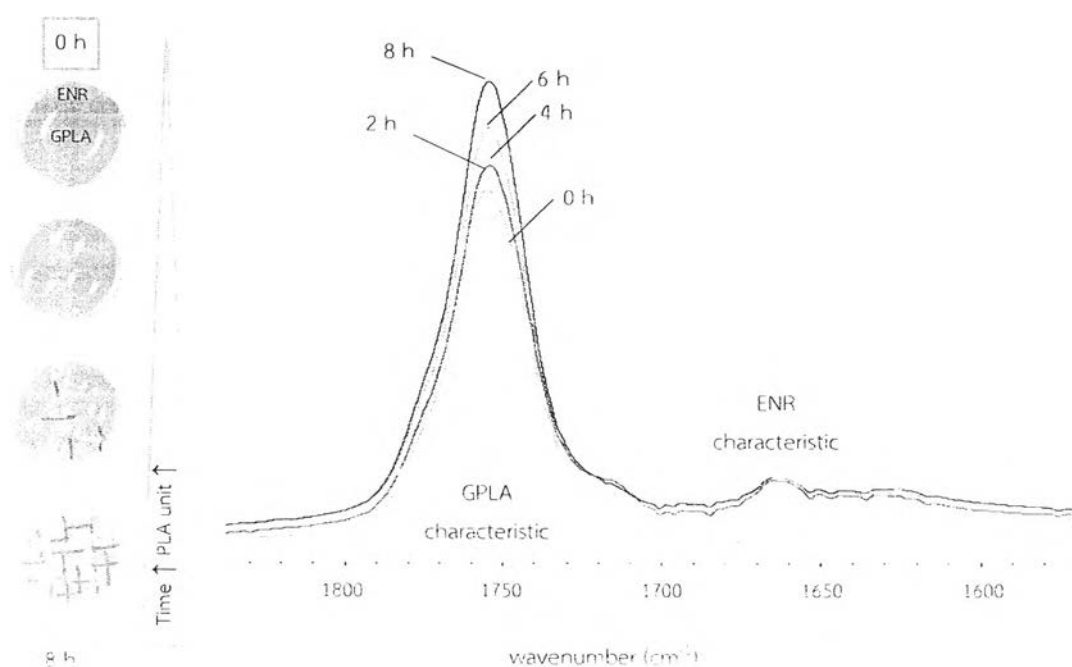


Figure 4.20 Normalized ATR-FTIR spectra of G10ER14, as a function of curing time.

For G44ER14, the intensity of the 1750 cm^{-1} mode seems to increase during the first two hours of the crosslinking reaction, as higher hydrophobicity of longer GPLA chain in non-polar rubber domains promotes better dispersion. After that, the LA signal decreases in intensity with an increase in the reaction time (Figure 4.21).

Entanglement of high molecular weight polymer chains and a phase separation of G44 from ENR occur with the progress of the crosslinking reaction.

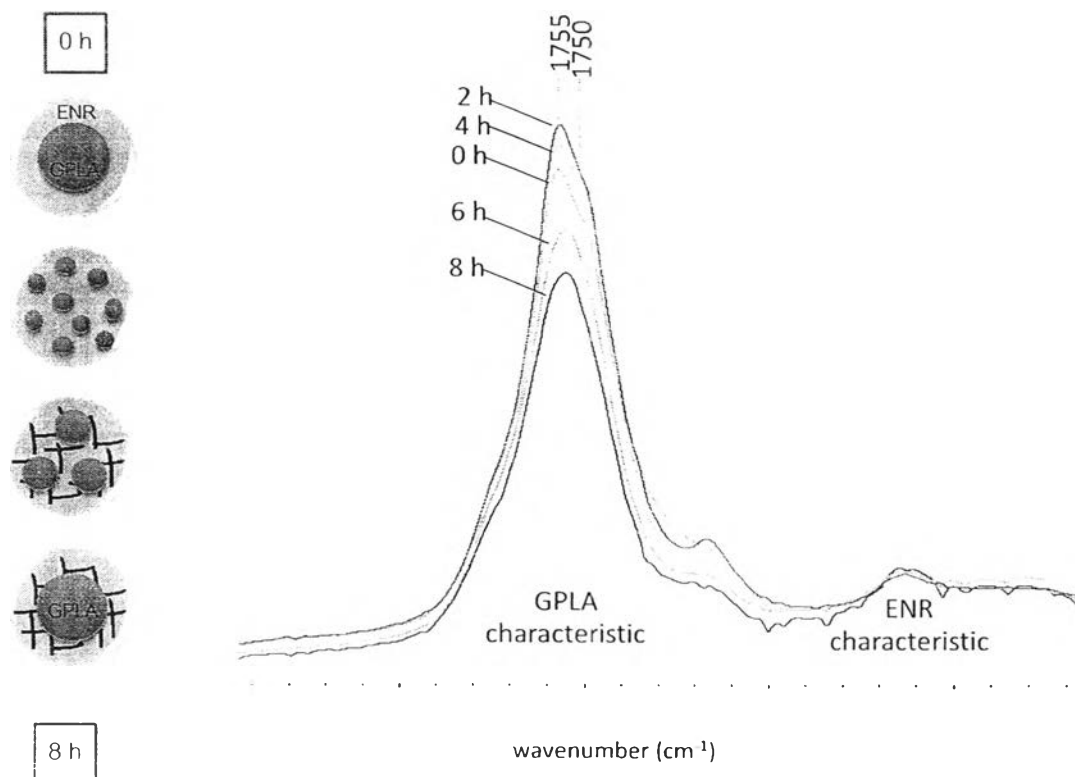


Figure 4.21 Normalized ATR-FTIR spectra of G44ER14, as a function of curing time.

Figure 4.22 show FTIR spectra of G2ER14. Two separate C=O signals are observed at 1750 and 1755 cm^{-1} , due to hydrogen bonded carbonyl with the relatively high content OH groups of the low MW G2. The intensity of the LA signals is decreased with and increasing of reaction time. This is caused by a high chain mobility of G2, which leads to rapid dispersion and crosslinking with epoxide groups, where as unreacted G2 is trapped in ENR matrix.

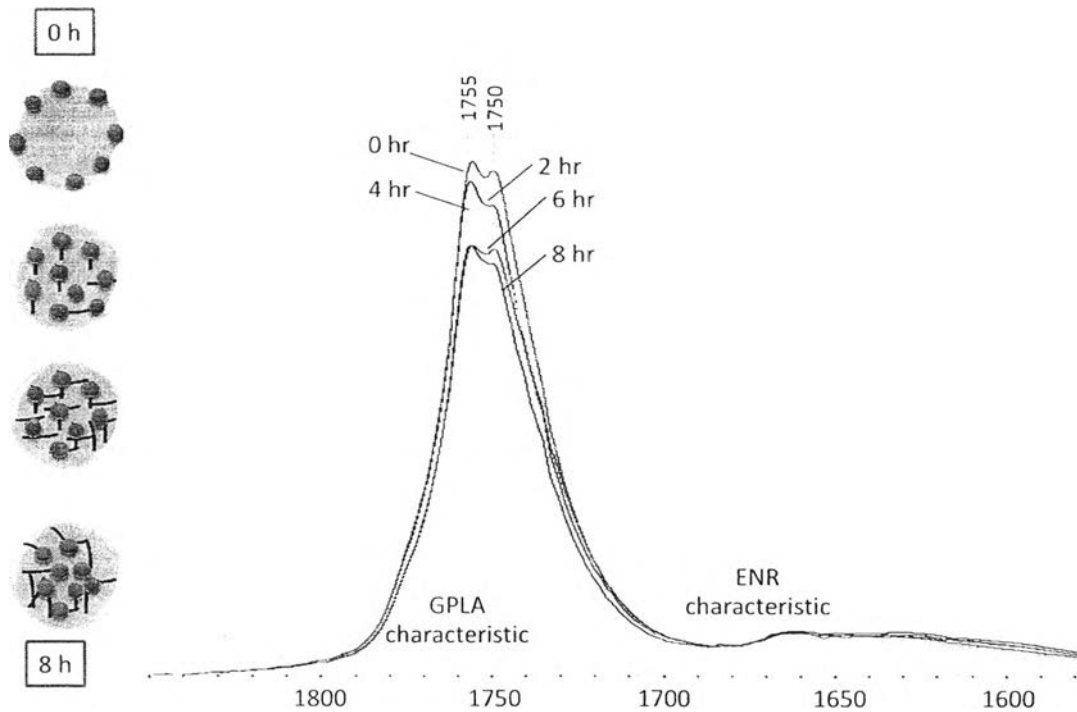


Figure 4.22 Normalized ATR-FTIR spectra of G2ER14, as a function of curing time

4.2.2.2. Crosslinking efficiency of GER products

Results on sequential extractions of GPLA-cured ENR samples by chemical crosslinking reactions (GER) are summarized in Figure 4.23

Figure 4.23 and Table 4.5. The weight contents of I_{-G1} is ranging from 14-50 %, while the corresponding values for S_{T21} and S_{THF} are about 1-39 wt% and 21-86 wt%, respectively. The content of the “grafted” fraction of G2-cured ENR is lower than those of G10 and G44, leading to higher gel content (93-98%). This reflects their higher crosslinking efficiency, which is corresponding to probability of the two hydroxyl groups to react with epoxide and form crosslinked junctions. The small-sized G2 molecules prefer to generate crosslinked structure, because of their high chain mobility (T_g is -10 °C), compared to the bigger sized counterparts. At the same size of G10ER and G2ER samples, the “crosslinked” structure is increased with and increasing of GPLA feed content, due to a relatively higher content of OH group.

However, G44ER11 shows less “crosslinked” structure than those of G44ER12 and G44ER14. This result causes by chain entanglement of G44, lead to phase separation of GPLA in ENR matrix.

The toluene-insoluble samples obtained from cured products of GPLA with moderate chain lengths (G10) possess the highest degree of swelling (2000-4000%). These results support our proposed crosslinking mechanisms that G10 chains act as long-chain bridges, which provide higher flexibility for the rubber network swelling. However, G44-cured samples show much lower degree of swelling (~10 folds), compared to G10-cured samples. This is likely due to chain entanglement of the longer polymer bridges, and partly the poor solubility of PLA sequences in toluene solvent as a result from the mismatch in their solubility parameters.

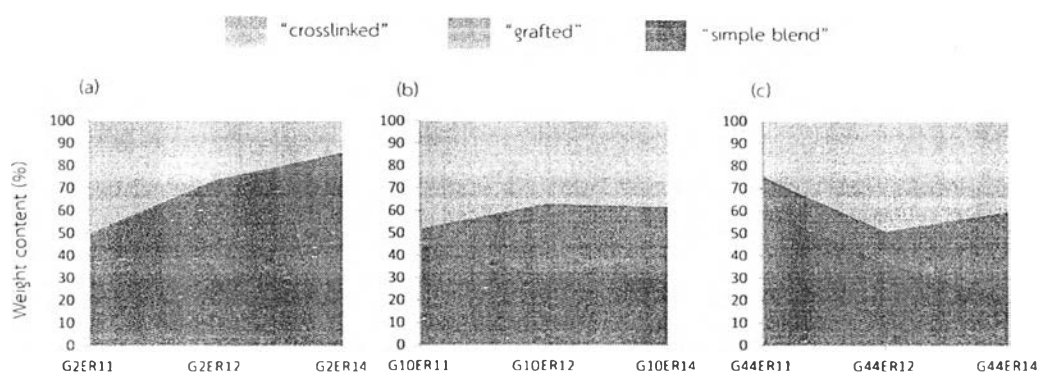


Figure 4.23 Weight content of each extracted fractions obtained from sequential solvent fractionation of G2ER (a), G10ER (b), and G44ER (c) cured samples.

Table 4.5 Weight contents of each extracted fraction obtained from sequential solvent fractionation, degree of swelling, and gel contents of GPLA-cured ENR products from chemical crosslinking reaction.

Samples	Weight fraction (%)			Swelling (%)	Gel content (%)
	THF soluble [S _{THF}]	Toluene soluble [S _{Tol}]	Toluene insoluble [I _{Tol}]		
G2ER11	49±4	3±4	48±2	426±8	93±6
G2ER12	72±5	2±2	26±3	387±7	93±5
G2ER14	83±2	0±0	17±3	492±11	100±2
G10ER11	44±4	7±1	48±3	2090±9	87±1
G10ER12	31±5	33±1	36±6	4283±8	52±5
G10ER14	41±6	23±4	37±2	3593±12	62±4
G44ER11	61±2	16±3	23±5	356±6	59±3
G44ER12	38±4	16±3	49±7	372±8	75±4
G44ER14	22±4	38±2	41±6	201±10	52±1

4.2.3. GPLA-cured ENR via reactive crosslinking (GET)

4.2.3.1. Chemical structures of GET products

FTIR spectra of G44ET14 mixtures before and after crosslinking in MDR, are compared with their starting materials (ENR and G44) in Figure 4.24. Characteristic signals of G44 are observed at 1750 (C=O stretching of lactate), 1185–1090 (C-O stretching of lactate), and 1045 cm⁻¹ (C-O bending of hydroxyl end group) [73]. The characteristic bands of ENR are observed at 3030 (C-H stretching of epoxide), 1655 (C=C stretching), 1375 (C-H symmetric deformation of -CH₃), 1255 (C-O stretching of epoxide), 875 (asymmetric stretching of epoxide ring), and 840 cm⁻¹ (C-H asymmetric stretching of CHR=CCR) [7, 69]. A mixture of ENR and GPLAs before crosslinking

exhibits the band characteristics of the 2 components, whose band intensity follows linear addition. The spectrum of cured G44ET14, obtained from a reactive blending process and a different spectrum of cured G44ET14 and G44ET14 mixture shows a negative intensity at 1375-1445 cm^{-1} , indicating a reduction of C-C stretching signal of rubber. Increasing of C-O-C signal is also shown at 1085 cm^{-1} , as a result of the ring-opening reaction of epoxide groups with hydroxyl groups of G44, achieved by catalyst, mechanical force and temperature.

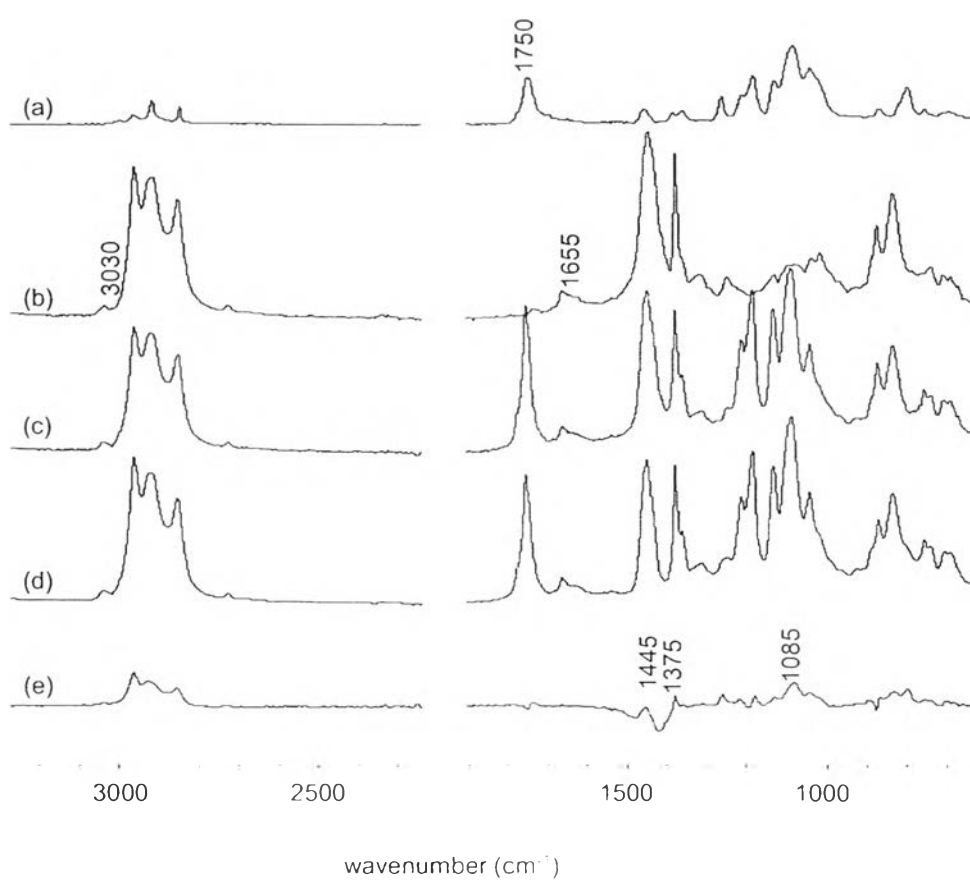


Figure 4.24 FTIR spectra of G44 (a), ENR (b), G44ET14 mixture (c), cured-G44ET14 (d), and different curve of cured-G44ET14 and G44ET14 mixture (e).

The relative intensity ratio of cured ENR samples generated from different ENR/G44 contents, are examined from normalized FTIR spectra, as shown in Figure 4.25. Changes in relative intensities of rubber/lactate units, i.e., the ratio of the 1375/1360, and 1655 / 1750 cm^{-1} bands, are observed. In the samples with high GPLA contents, the relative intensity of rubber units (1375 and 1655 cm^{-1}) decreases, while those of lactate units (1360 and 1750 cm^{-1}) increases. This result is agreed with the ENR/G44 compositions in feed.

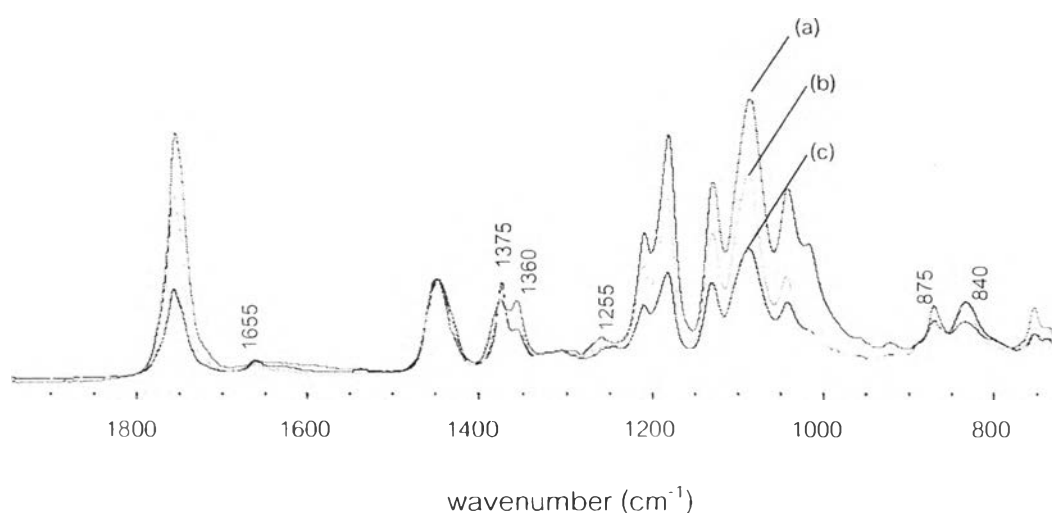


Figure 4.25 Normalized FTIR spectra of G44ET cured samples obtained at various compositions: G44ET11 (a), G44ET12 (b), and G44ET14-cured samples (c).

FTIR spectra of solvent-extracted products from all cured samples obtained from different feed compositions, as shown in Figure 4.26, reflect low intensity of the epoxide band at 1255 cm^{-1} . This confirms the occurrence of the ring-opening reaction in S_{T+E} and I_{T+E} fractions. On the other hand, the corresponding spectrum of S_{T+E} shows intense bands of C-O stretching mode of lactate (1090-1185 cm^{-1}), C-O bending of hydroxyl end groups at 1202-1045 cm^{-1} , and a very sharp band of free epoxide ring at 1255 cm^{-1} . This indicates that the 2 blend components are largely mixed without chemical reaction.

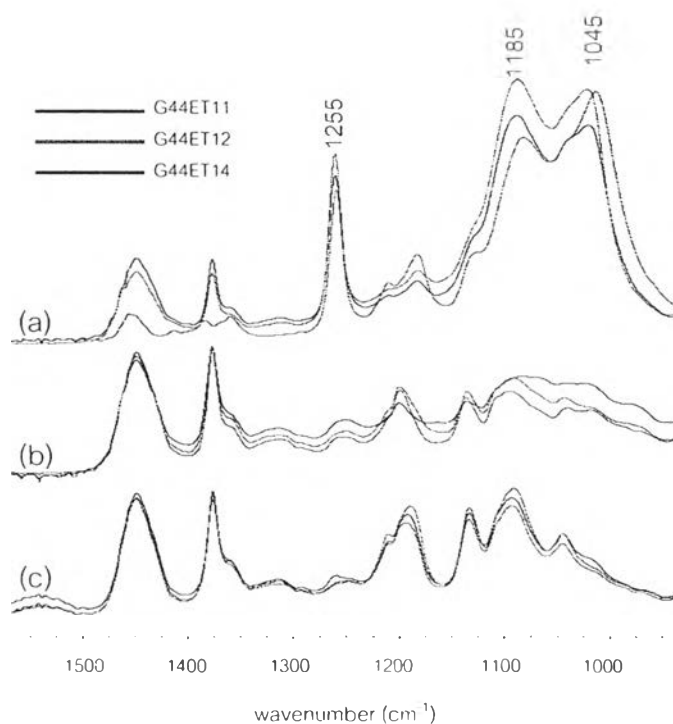


Figure 4.26 FTIR spectra of S_{THF} (a), S_{Tot} (b), and I_{Tot} fractions (c) of GPLA-cured ENR products generated from different feed contents.

Figure 4.27 shows ATR-FTIR spectra of THF-soluble fraction of all GPLA-cured samples. The spectra exhibit a domination of GPLA characteristics, reflecting a low content of unreacted ENR, as the majority of epoxides are reacted by OH-capped G2 to form “crosslinked” and “grafted” structures. In contrast, ENR band characteristics are observed in those of G10ET11, G44ET14, and G44ET11. This corresponds to excess and slightly-grafted ENR chains, as the feed OH/epoxide molar ratios of big-sized GPLA are lower. Also, lower chain mobility of the large GPLA molecules may retard their reaction efficiency. Information on chemical structures and interactions of the cured products are also derived from changes in band frequency of the C=O stretching mode. A typical frequency of the band for lactate of GPLA glycolysates is observed at 1750 cm^{-1} . After a reaction with ENR, a new band appears at 1755 cm^{-1} , as a result from the conversion of -OH end groups, leading to lower degree of

hydrogen bonding of the carbonyl groups. The intensity of the 1755 cm^{-1} band is dependent on the GPLA/ENR ratios, in which the higher ratio leads to a more intense band, and hence a higher degree of ring-opening reaction of the epoxide groups. Also, the more intense band is observed with the employment of small-sized GPLAs. This is in good agreement with those observed in other experiments.

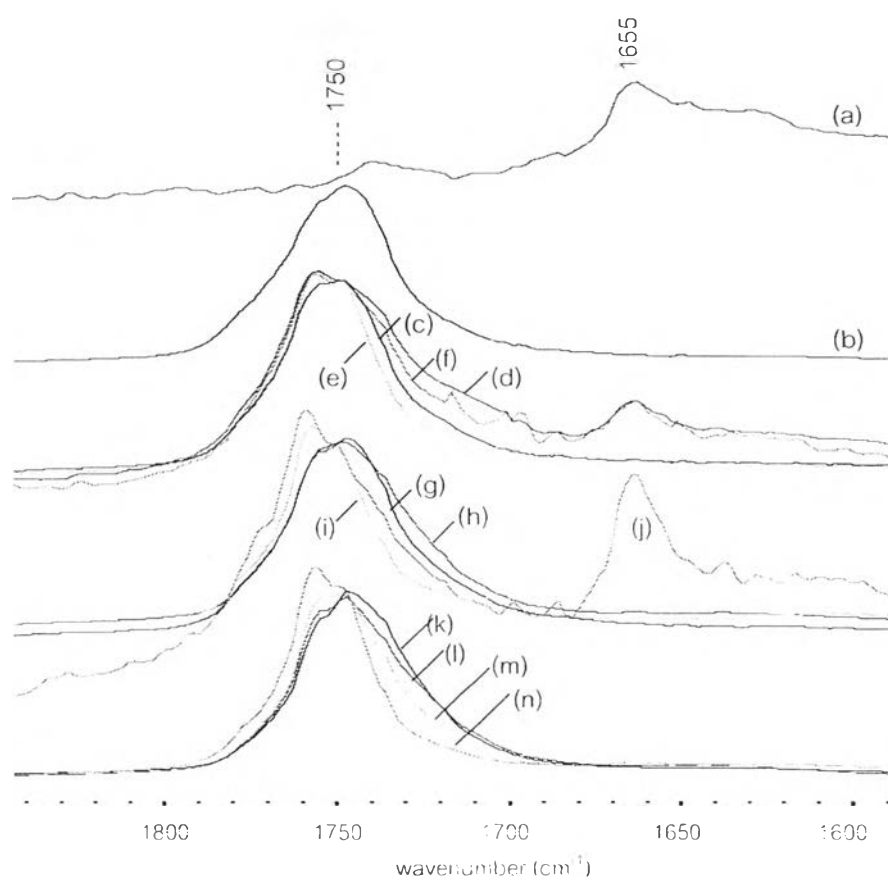


Figure 4.27 ATR-FTIR spectra of pure-ENR (a), cPLA (b), THF-soluble fraction of G44 (c), G44ET11 (d), G44ET12 (e), G44ET14 (f), G10 (g), G10ET11 (h), G10ET12 (i), G10ET14 (j), G2 (k), G2ET11 (l), G2ET12 (m), and G2ET14 (n).

The “crosslinked” structure is confirmed by the presence of lactate characteristics in FTIR spectra of toluene-insoluble fraction (I_{TOI}). Figure 4.28 shows normalized FTIR spectra with respect to the intensity of the C=C stretching mode.

The normalized band intensity of the C=O stretching mode of lactate varies with GPLA sizes and GPLA/ENR ratios. The samples prepared from high GPLA feed contents exhibit more intense band intensity, reflecting higher contents of GPLA crosslinkers. On the effect of size of GPLAs, it is observed that the cured ENR products obtained from G10 show relatively higher band intensity when the same feed ratio is employed. This indicates an optimum curing efficiency, which is in good agreement with results from other techniques.

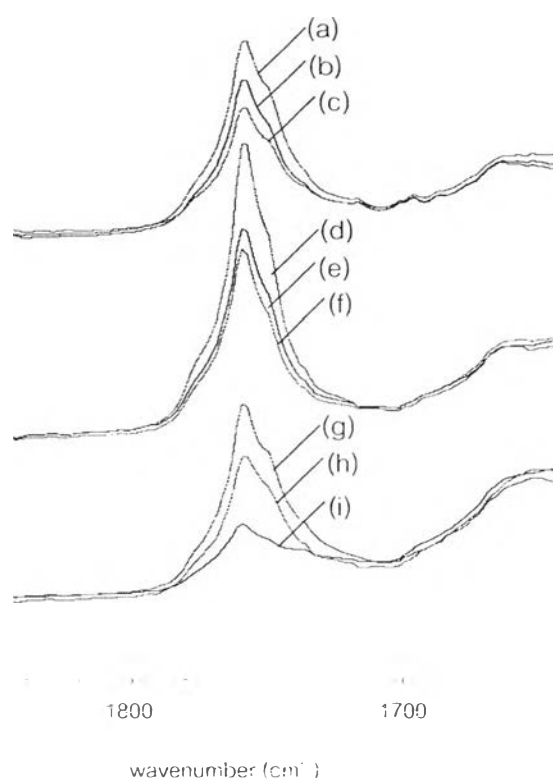


Figure 4.28 Normalized ATR-FTIR spectra of toluene-insoluble fraction of G44ET11 (a). G44ET12 (b), G44ET14 (c), G10ET11 (d), G10ET12 (e), G10ET14 (f), G2ET11 (g), G2ET12 (h), and G2ET14 (i).

4.2.3.2. Reaction efficiency of GET products

Results from sequential extraction of GPLA-cured ENR samples generated from a reactive crosslinking process are summarized in Figure 4.29 and Table 4.6. The weight content of I_{Tot} is ranging from 16-39 %, while the values for S_{Tot} and S_{THF} are 10-42 and 41-71 %, respectively. The crosslinking of ENR by this reactive blending in MDR for 30 min also produces cured products with 3 fractions, i.e., “crosslinked”, “grafted”, and “simple blend”. The gel contents of these products are significantly lower than those from chemical curing reaction method, due to shorter reaction time and limitation of chain movement and flexibility in melt state compared to solution. In contrast, an increase in the content of “grafted” fraction is observed in G2 and G10 cured ENR samples. This is probably because small-sized GPLAs contain a high number of -OH end groups, leading to higher probability of single end-group reaction with ENR in early stage of crosslinking (less than 30 min). For the cured products prepared from the same feed compositions, a content of “crosslinked” fraction (I_{Tot}) increases with GPLA chain lengths. When the same GPLA is employed, a high content of “crosslinked” structure is obtained from the application of 1:4 and 1:2 GPLA:ENR weight ratios, which determines an optimum relative OH/epoxide ratios of the curing reaction. These results strongly indicate that the reactive blending method is effective for polymeric-crosslinking of ENR.

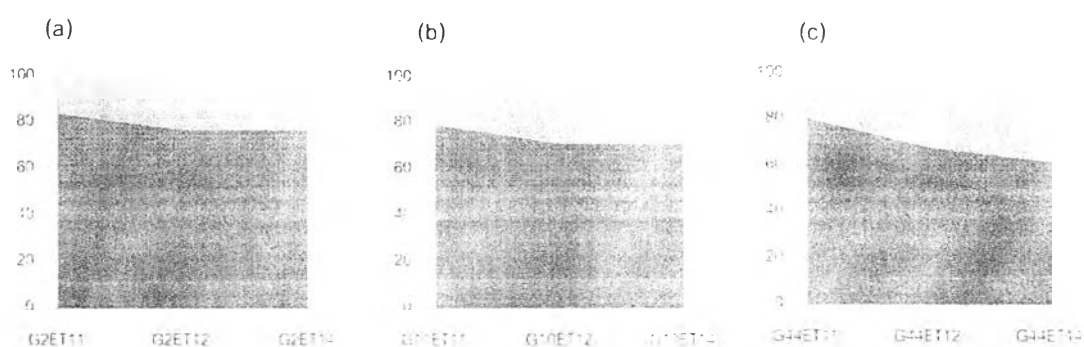


Figure 4.29 Weight content of each extracted fractions obtained from sequential solvent fractionation of G2ET (a), G10ET (b), and G44ET (c) cured samples.

เลขหมาย..... ๐๗- 2756
 เลขทะเบียน..... 7193
 วันเดือนปี..... 6 มี.ค. 2560

Table 4.6 Weight contents of extracted product obtained from sequential solvent fractionations, degree of swelling, and gel contents of the cured ENR materials prepared from a reactive crosslinking method.

Samples	Weight fraction (%)			Swelling (%)	Gel content (%)
	THF soluble [S _{THF}]	Toluene soluble [S _{Tol}]	Toluene insoluble [I _{Tol}]		
G2ET11	55±2	29±3	16±3	2484±7	35±3
G2ET12	60±3	17±3	23±4	4022±10	58±4
G2ET14	42±4	34±2	23±3	1834±8	40±5
G10ET11	38±3	42±1	21±3	2063±7	33±2
G10ET12	49±5	22±2	29±5	3438±6	57±4
G10ET14	45±4	27±2	29±2	3739±10	52±5
G44ET11	71±3	10±3	20±3	1273±9	67±3
G44ET12	56±2	12±3	32±5	1594±12	73±3
G44ET14	41±2	21±2	39±4	1648±10	65±2



4.2.4. Effects of GPLA content and GPLA molecular weight on crosslinking behaviors

Curing behaviors of compounding GPLA/ENR materials are investigated by MDR, where the plots of torques required to oscillate the samples as a function of curing times are examined, as shown in Figure 4.30. The elastic torque, which represents the degree of crosslinking is proportional to the stiffness or shear modulus of the rubber specimens. In the curing reaction of neat ENR, the elastic torque reaches a constant value at 125 N/m. The corresponding data for all GPLAs/ENR mixtures show a sudden increase in the values during the first 5 min of curing time, because of the increase in the degree of crosslinking. This indicates that scorch times for this curing mechanism is shorter than 5 min, which is similar to those of typical sulfur-vulcanized rubber materials (~2 min) [69]. The crosslinking efficiency is determined from the sample elasticity, where the cured-ENR network obtained from a high-MW crosslinker (G44) shows an increase in elasticity with an increase of the G44 loading content. It is noted that the increase in elastic torque of the samples is partly due to the higher values of the GPLA plastic domain. In contrast, when smaller GPLA crosslinkers (G10 and G2) are used, the samples with lower GPLA feed contents show higher elasticity, due to a higher probability of reaction between -OH groups and epoxides. Also, the contribution of elastic torque from smaller-sized GPLAs is lower.



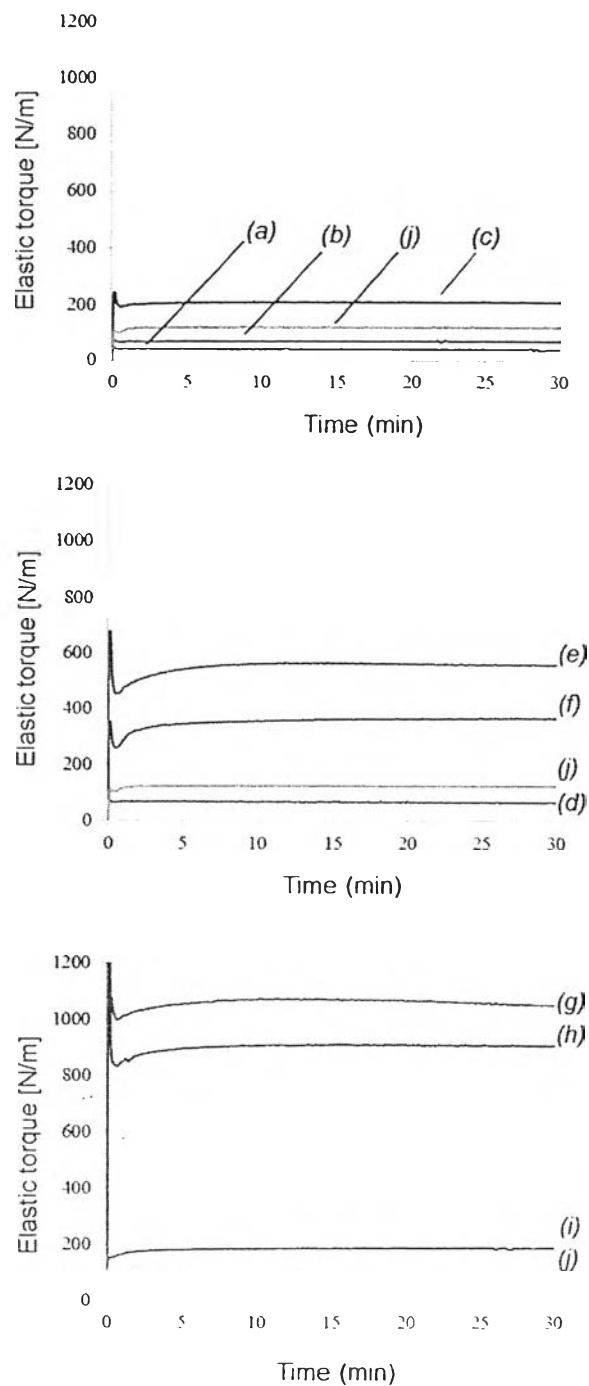


Figure 4.30 Elastic torque vs. time curves of G2ET11 (a), G2ET12 (b), and G2ET14 (c) G10ET11 (d), G10ET12 (e), G10ET14 (f), G44ET11 (g), G44ET12 (h), G44ET14 (i), and pure-ENR (j).

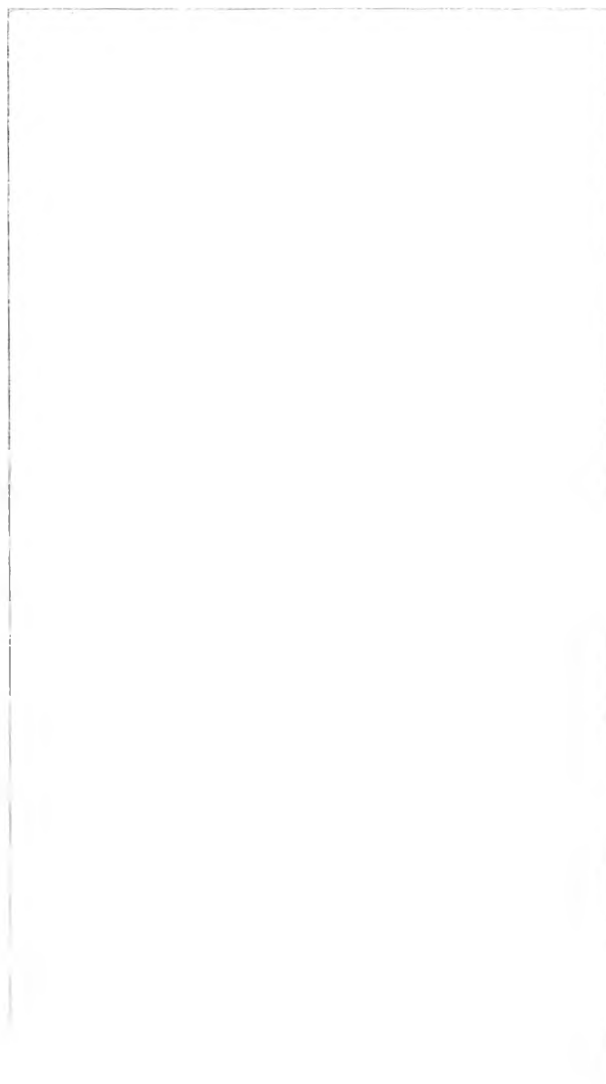


Figure 4.31 Crosslinking characteristics, in terms of elastic/viscous torque and $\tan \delta$, of G2/ENR (a), G10/ENR (b), and G44/ENR mixtures (c), as a function of GPLA contents.

The excess (unreacted) ENR and GPLA chains affect the flow behaviors of the samples, as reflected in the sample viscous torques. The curing reaction of ENR by G44 shows a gradual increase in viscous torque (Figure 4.31), due to high content of excess GPLA and ENR. In contrast, an employment of G2 and G10 crosslinkers leads to a slight increase in the value, as their high -OH contents leads to higher crosslinking and grafting efficiencies. The ratio of damping to elasticity behaviors of the samples is reported in terms of a loss tangent ($\tan \delta$). Figure 4.31 shows that all GPLA/ENR mixtures have lower $\tan \delta$ values than neat ENR. As the low values represent high crosslinking ability, this confirms that G44, G10, and G2 are successfully used as crosslinkers for ENR. The lowest $\tan \delta$ values, in all GPLAs systems is observed when a 33 wt% of GPLAs is employed. This reflects a larger contribution of crosslinking characteristics than the “simple mixture” behaviors, which indicates that these are optimum feed compositions.

4.2.5. Tensile properties of GPLA-cured ENR materials.

According to the results from cured ENR products obtained from a reactive blend in MDR, a suitable GPLA/ENR weight ratio of 1:2 is observed for curing in a melt state. Therefore, mechanical properties of the samples prepared from these conditions are examined. However, samples obtained from MDR experiments are not suitable for the tests. Therefore, films for tensile tests were prepared by hot pressing the GPLA/ENR blends, which were compounded in an internal mixer (according to 3.6.5).



Table 4.7 and Figure 4.32 show tensile properties of GPLA-cured ENR products, generated from GPLA with different molecular weight. A GPLA:ENR ratio of 1:2 is employed. After the curing reaction in an internal mixer at 80°C, an increase in tensile strength, modulus, elongation at break and breaking energy of GPLA-cured ENR materials is observed. Tensile strength and breaking energy increase with increasing of GPLA molecular weight, as the crosslinked network is formed. Excellent elongation at break is obtained in G2ET12 and G44ET12 samples. On the other hand, G10ET12 exhibits the highest modulus. This indicates that the high content of “simple blend” fraction in G2ET12 ENR (60%) and G44ET12 (56%) is a major cause for compatibility enhancement of the crosslinked rubber domains, whereas PLA matrix and “grafted” and “crosslinked” fractions act as hard phase for modulus improvement, as illustrated in Figure 4.33.

Table 4.7 Tensile properties of GPLA-cured ENR with GPLA at various molecular weights.

Samples	Tensile strength (MPa)	Elongation at break (%)	Modulus (MPa)	Break Energy (10^{-9} J/m ²)
uncured ENR	0.26±0.01	117±34	0.79±0.00	11±40
G2ET12	0.59±0.26	347±119	0.44±0.12	62±39
G10ET12	0.78±0.02	306±16	9.51±1.41	88±19
G44ET12	1.47±0.21	419±79	3.09±0.97	170±30

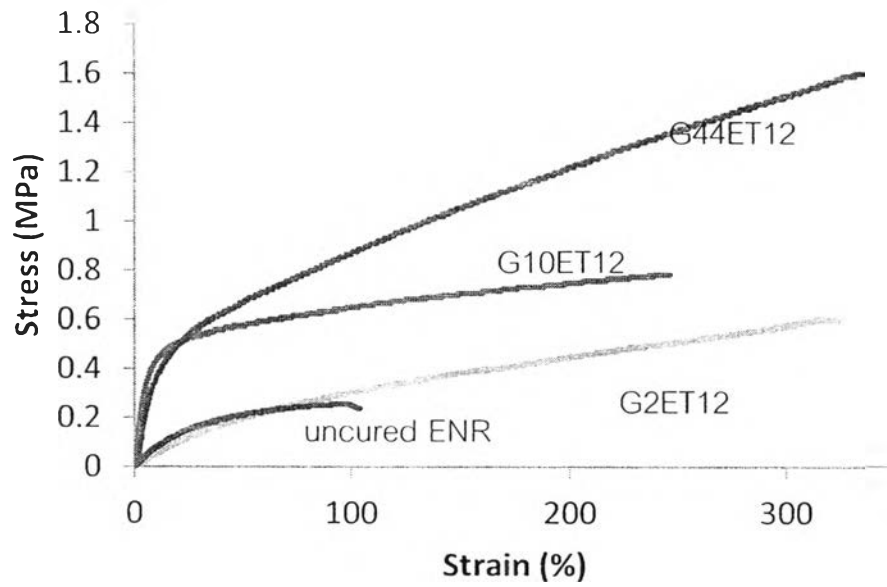


Figure 4.32 Stress-strain curves of GPLA-cured ENR products obtained from GPLAs with different molecular weights.

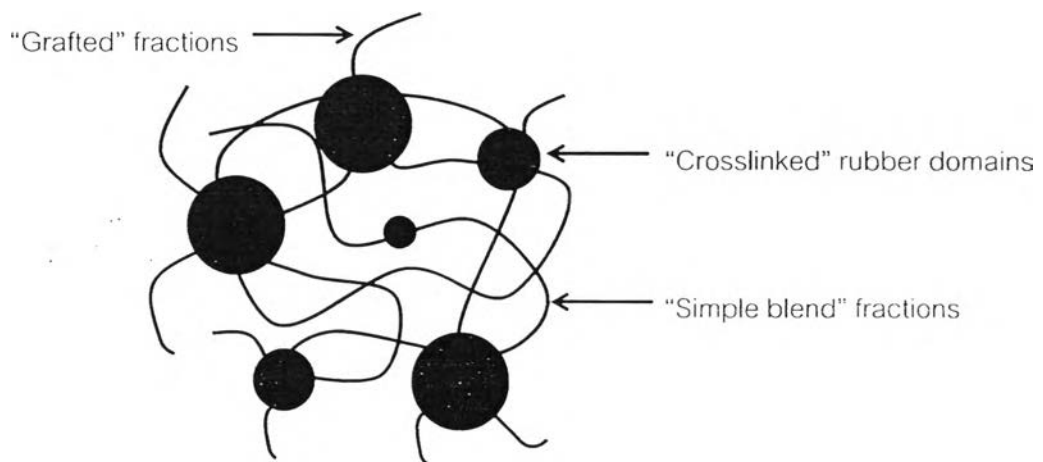


Figure 4.33 Proposed morphology of GPLA-cured ENR materials.

4.2.6. Thermal properties and weight compositions of GPLA-cured ENR products

TGA and DTGA thermograms of GPLA-cured ENR products produced from a reactive crosslinking process are shown in Figure 4.34-4.36. Thermal decomposition of pure GPLA and ENR involves a one-step degradation mechanism. It is noted that neat ENR (20 mol% epoxide content) exhibits a slight weight loss mechanism in the 90-250 °C temperature range [74], which are likely due to a removal of residual solvents (water and THF) and probably an epoxide ring-opening reaction, which takes place during the analysis.

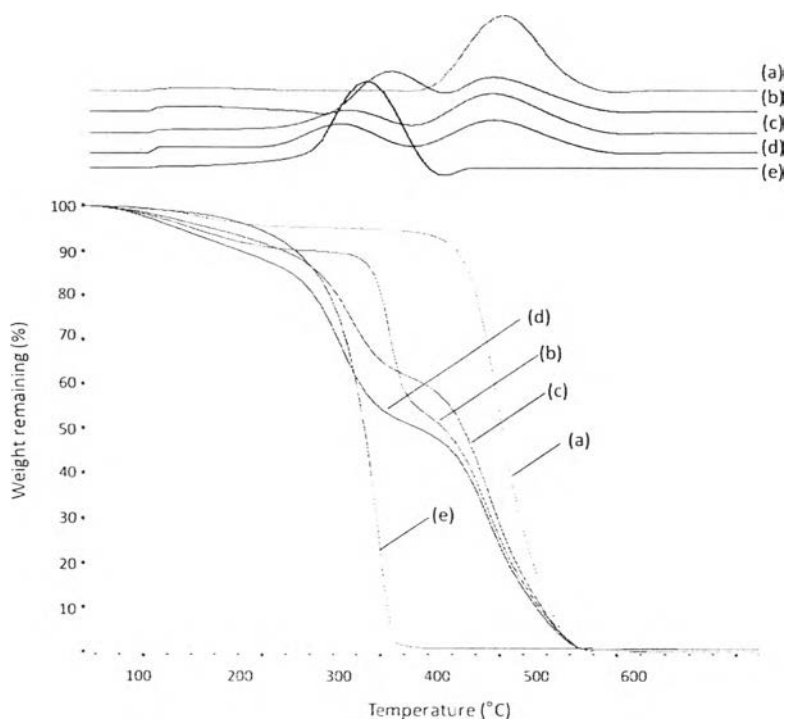


Figure 4.34 TGA and DTGA curves of neat ENR (a), cured G2ET14 (b), cured G2ET12 (c), cured G2ET11 (d), and pure G2 (e).

All 3 cured ENR samples show decompositions of lactate sequences in the 200-400 °C range, whereas that of neat ENR is observed at 400-500 °C. The content of lactate and ENR components are determined from the corresponding percentage weight loss. As lactate sequences in free GPLA chains are degraded at 180-300 °C, whereas that of the “crosslinked” lactate units is observed at 350 °C, the contents of crosslinked GPLA in the samples are calculated, where the values of 14-48 % are

observed (Table 4.8). The highest crosslinking efficiency is observed in G44ET12, whereas the lowest is found in G2ET11. This is in good agreement with results on $\tan \delta$ values, as discussed earlier. This reflects that chain mobility of GPLA plays an important role in the crosslinking reaction. As G2 has the smallest size with the highest mobility (T_g -10 °C), so that this produces “grafted” and “unreacted” fractions more than the “crosslinked” structure. In contrast, $-OH$ groups of the more rigid GPLAs, i.e., G10 (T_g 52 °C) and G44 (T_g 60 °C) are more reactive with epoxide groups, leading to higher contents of polymeric bridges between ENR chains.

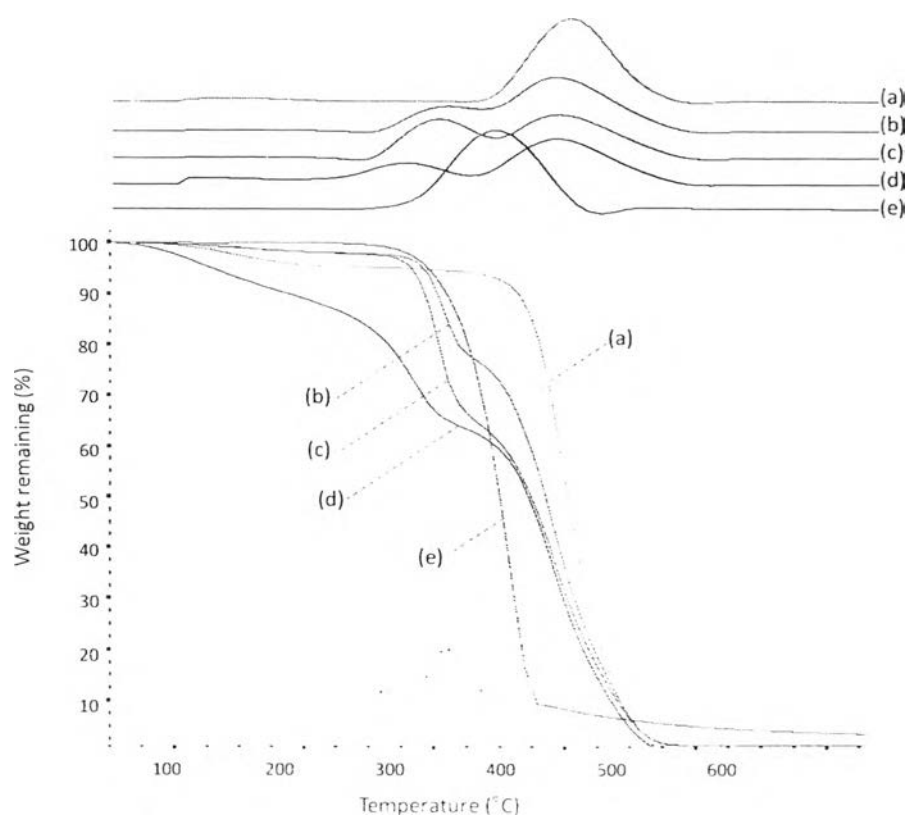


Figure 4.35 TGA and DTGA curves of neat ENR (a), cured G10ET14 (b), cured G10ET12 (c), cured G10ET11 (d), and pure G10 (e).

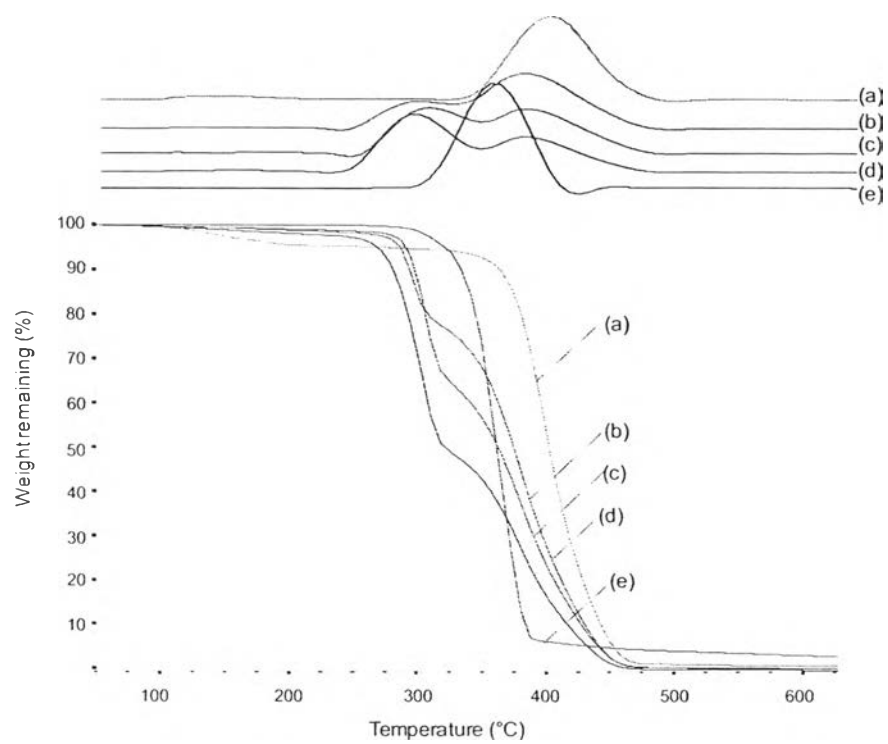


Figure 4.36 TGA and DTGA curves of neat ENR (a), cured G44ET14 (b), cured G44ET12 (c), cured G44ET11 (d), and pure G44 (e).



Table 4.8 Thermal degradability of cured ENR samples prepared from various GPLA/ENR compositions and GPLA molecular weights.

Samples		LA domains		LA-crosslinked	ENR domains	
				junction		
G2ET11	Temp (°C)	180	280	350	400	450
	wt. %	12	34	14	36	4
G2ET12	Temp (°C)	180	275	350	400	430
	wt. %	9	35	16	43	5
G2ET14	Temp (°C)	180	300	350	410	425
	wt. %	9	13	35	38	5
G10ET11	Temp (°C)	180	250	350	400	450
	wt. %	11	5	34	45	3
G10ET12	Temp (°C)	180	250	350	400	430
	wt. %	2	18	29	44	7
G10ET14	Temp (°C)	180	250	350	400	425
	wt. %	2	9	29	53	6
G44ET11	Temp (°C)	200	300	350	400	450
	wt. %	2	49	17	25	7
G44ET12	Temp (°C)	200	290	350	400	430
	wt. %	1	14	48	27	10
G44ET14	Temp (°C)	200	290	350	410	425
	wt. %	2	22	31	33	12



3475981822

4.3. GPLA-cured ENR products as a toughening agent for PLLA resins

4.3.1 Tensile properties of GPLA-cured ENR/PLLA blends

GPLA-cured ENR products possess excellent characteristics as a toughening agent for commercial PLLA resin, since the materials contain flexible cured-rubber domains and lactate sequences, which are compatible with PLLA resin. The materials are, therefore, blended with PLLA resin at various compositions. Tensile properties of the blends are shown in Figure 4.37-4.40. Figure 4.37 show that tensile strength of pure PLLA is 36.2 MPa. An incorporation of uncured ENR and G2-cured ENR leads to a decrease in the value.

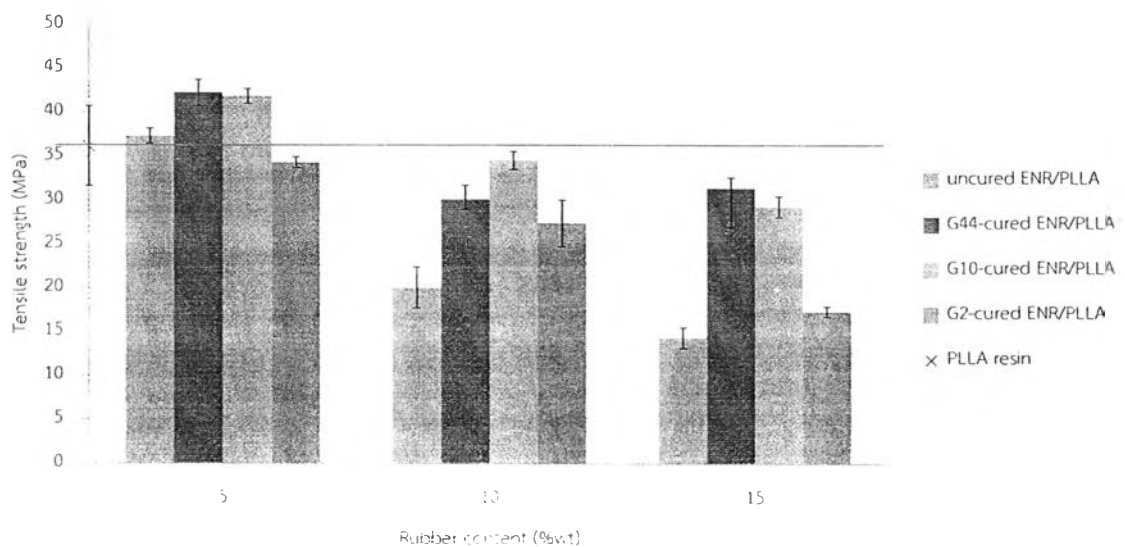


Figure 4.37 Tensile strength of GPLA-cured ENR/PLLA blended samples at various blend compositions.

The reduction is also dependent on an increase of the rubber contents, from 5 to 15 %wt due to the rubbers low strength. In contrast, an application of G44-cured ENR and G10-cured ENR results in higher tensile strength, compared to those of G2-cured and uncured ENR blends at the same compositions. In fact, at 5 %wt content the blend containing G10-cured ENR and G44-cured ENR exhibit slightly improvements in tensile

strength. This is likely because of the relatively higher contents of “crosslinked” structure imposes strong effect on tensile strength of the blend materials.

For typical rubber/polymer blends, modulus of the blends decreases with an increase in the rubber contents. Figure 4.38 shows that modulus of all cured ENR/PLLA blend with 5%wt of rubber content is comparable to that of pure PLLA resin, due to the low content of rubber phase. Upon increasing of the rubber content a decreasing trend of the modulus is observed. However, the use of 10-15 %wt of G10 and G2-cured ENR products leads to an increase of the modulus, because of their higher contents of the “grafted” fraction, compared to that of the G44-cured ENR counterpart.

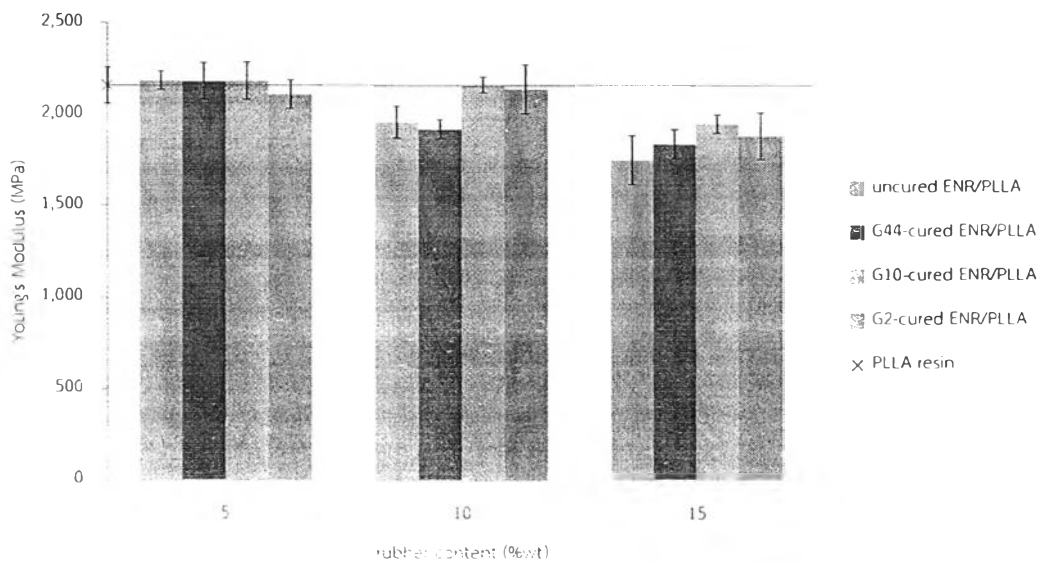


Figure 4.38 Young's modulus of GPLA-cured ENR/PLLA blended samples at different blend compositions.

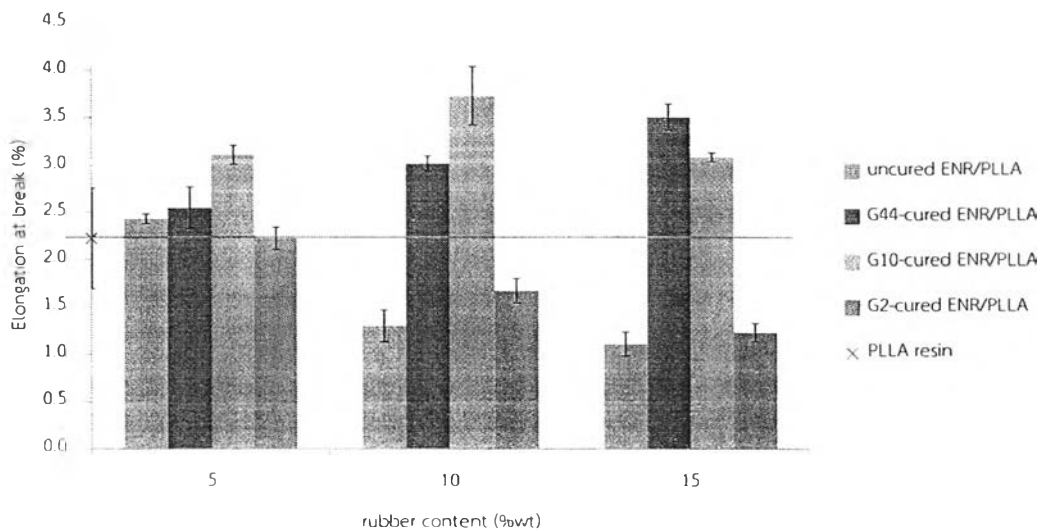


Figure 4.39 Elongation at break of GPLA-cured ENR/PLLA blended samples at different blend compositions.

With an incorporation of uncured ENR and G2-cured ENR products, the elongation at break of the blend samples decreases, whereas those consisting of G10-cured ENR and G44-cured ENR slightly increase, as shown in Figure 4.39. It is believed that the difference in elongation at break is dominated by the plastic deformation behaviors of the materials. This explanation is confirmed from this experiment, in which blends of G10-cured ENR and G44-cured ENR samples show larger plastic deformation zones near the fracture flank, compared to those containing uncured ENR and G2-cured ENR. This agrees well with a report from other study [4], and is also in good agreement with the results on breaking energy of the blends, as summarized in Figure 4.40.

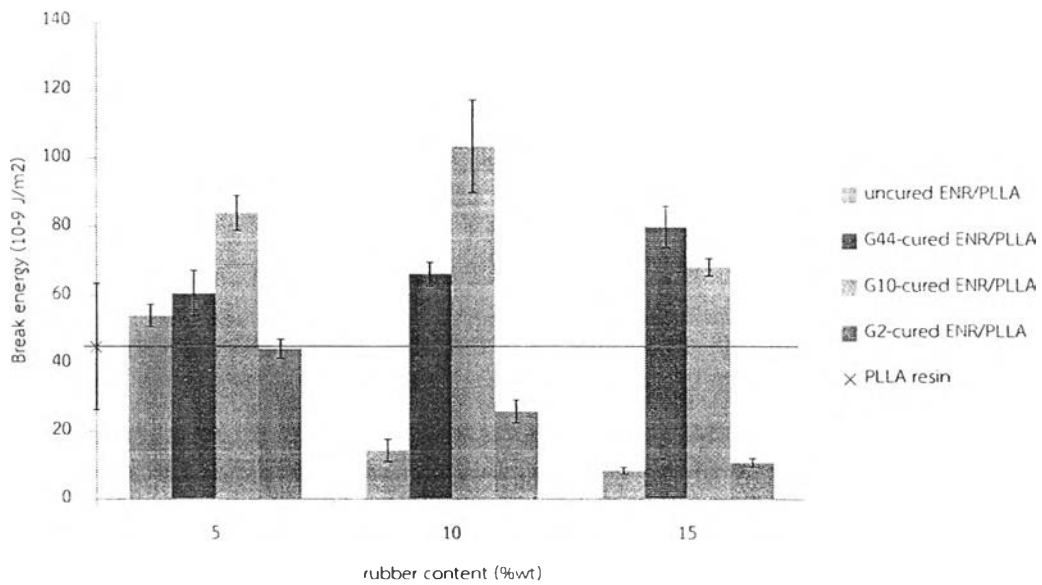


Figure 4.40 Breaking energy of GPLA-cured ENR/PLLA blended samples at various blend compositions.

4.3.2. Impact strength of GPLA-cured ENR/PLLA blends

Results on the Izod impact strength of all blend samples are shown in Figure 4.41. Only G44-cured ENR/PLA blend shows higher impact strength than pure PLLA film at all blend compositions. Morphology of the fracture samples are examined by SEM micrographs, as shown in Table 4.9. It was reported that an improvement in impact strength was most likely attributed to smaller rubber particle size in PLLA matrix [4]. In this study, G44-cured ENR/PLLA blend exhibits the smallest rubber particle size (2-3 μm), and also shows fibrillation of PLLA matrix during breaking. It is concluded that G44-cured ENR material has high efficiency in toughening of PLLA resin due to its grafted structure which consists of effective long GPLA branch. However, an incorporation of uncured ENR and G2-cured ENR (15%wt) products leads to an apparent decrease in impact strength, due to formation of large voids in the matrix. Flocculated morphology of rubber is also observed and large voids thereby are created (15 μm for 15%wt G2-cured ENR). This

suggests that the fracture crack run along the interface between the PLLA matrix and the rubber particles. The contents of voids observed in the samples clearly increases with the rubber contents for all blend samples, leading to their lower impact strength.

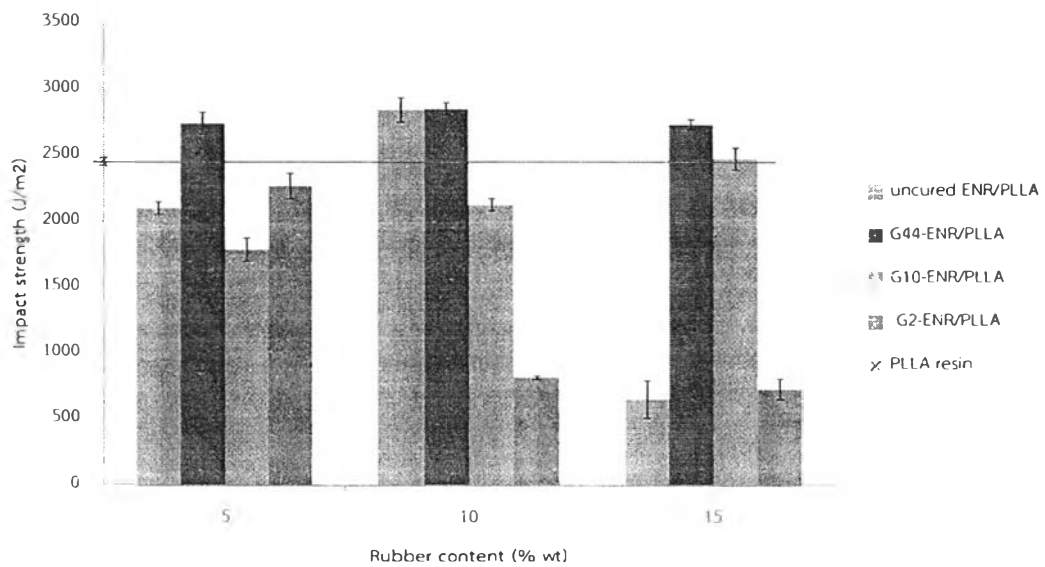
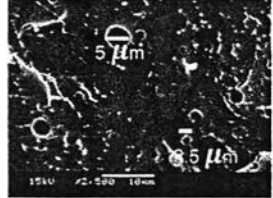
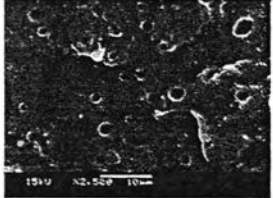
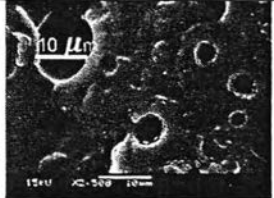
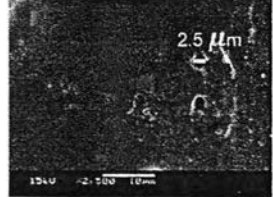
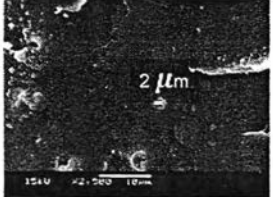

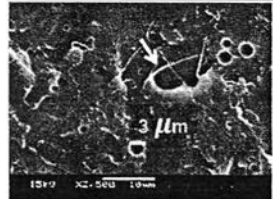
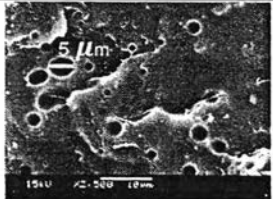
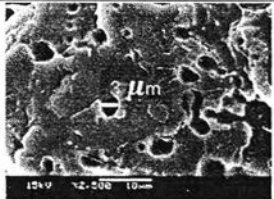


Figure 4.41 Impact strength of GPLA-cured ENR/PLA blended samples at various blend compositions.

Table 4.9 SEM micrographs of GPLA-cured ENR PLLA blends using different GPLA at various blend compositions.

Toughening agent	5%	10%	15%
Uncured ENR			
G2ET12			
G10ET12			
G44ET12	